We are IntechOpen,
the world's leading publisher of
Open Access books
Built by scientists, for scientists

4,800
Open access books available

122,000
International authors and editors

135M
Downloads

Our authors are among the

154
Countries delivered to

TOP 1%
most cited scientists

12.2%
Contributors from top 500 universities

CLARIVATE ANALYTICS

BOOK CITATION INDEX

INDEXED

WEB OF SCIENCE™

Selection of our books indexed in the Book Citation Index
in Web of Science™ Core Collection (BKCI)

Interested in publishing with us?
Contact book.department@intechopen.com

Numbers displayed above are based on latest data collected.
For more information visit www.intechopen.com

Design, Manufacture and Performance Evaluation of Non-Asbestos Sealing Composites

Boqin Gu, Ye Chen and Jianfeng Zhou
Nanjing University of Technology,
China

1. Introduction

Asbestos was once considered to be a "miracle mineral". This naturally occurring silicate has many desirable characteristics, including resistance to fire, heat, and corrosion. It is strong, durable and flexible. Asbestos is inexpensive because it is available in abundant quantities. Its versatility has led to its use as a component of a variety of products in numerous industries (American Academy of Actuaries, 2007). The development of fiber-reinforced elastomer gaskets began in the 1880s and led to the patent application for Klingerit in 1904 (Piringer & Rustemeyer, 2004). Since more than one hundred years ago, these kinds of non-metallic gaskets, which were made of compressed asbestos fibers (CAF) materials, have been the most widely used sealing elements with a maximal yield.

Up till the 1970s, the health hazards of asbestos were recognized. Several diseases have been linked to asbestos exposure, including mesothelioma, lung cancer, other cancers, asbestosis, and pleural changes (American Academy of Actuaries, 2007). Due to the restriction on the use of asbestos, the pressure was on scientists and engineers to develop non-asbestos gasket material replacements, and asbestos was replaced by alternative fibers and fillers. These alternatives were employed in an attempt to replicate the product properties of the former CAF materials. These substitutes were developed using reinforcing fibers like aramid, glass and carbon fibers to achieve high strength, and additives like inorganic materials (e.g., clays, precipitated silica, graphite etc.). Since the 1990s, a great number of worldwide famous sealing materials manufacturers have put significant efforts onto the development of a variety of novel non-asbestos sealing composites (NASC), such as Garlock in USA, Klinger in Austria, Kempchen in Germany, and Valqua and Pilar in Japan. Collaborating with some international organizations and research institutions, they conducted a series of experimental and application researches, and obtained many valuable results (Payne & Bazergui, 1990). These investigations have laid a foundation for further studies on performance evaluations and industrial applications.

Aramid was used as reinforcing fibers in the earliest non-asbestos gasket materials, because it provided processing advantages, especially during calendaring. However, it is very expensive and has poor thermal stability. Most commonly used fibers and fillers in non-asbestos gasket materials do not achieve the outstanding stability as CAF materials do when the binding elastomers become aged. More recently, novel formulations and manufacturing

processes have been developed based on cheap reinforcing fibers, the hybrid effect of different reinforcing fibers or an adapted material structure. These non-asbestos gasket materials not only are significantly cheaper but also have a better performance at high temperatures. Gu & Chen developed two kinds of sealing composite materials. One was reinforced with aramid and pre-oxidized hybrid fibers and prepared by molding preparation method and the other was reinforced with carbon and glass hybrid fibers and manufactured by using calendar preparation method. The effect of different surface treatment methods of the fibers on the heat resistance of the composite materials was studied. The optimum prescriptions of the composites were obtained by regression design method (Gu & Chen, 2007; Chen & Gu, 2008). Gao & Chen carried out explorative investigations on the preparation method of nanometer calcium carbonate filled modifications of rubber-based sealing composite materials and on the influence of nanometer filled modifications on the mechanical properties of the prepared gasket materials (Gao & Chen, 2009). A novel material concept for compressed fiber materials was proposed to significantly decelerate the ageing of elastomer bound gasket materials by the use of special elastomers and an adapted material structure, i.e., the multi-layer structure. The steam testing, as opposed to the standard gasket testing, has been used to demonstrate this improvement (Piringer & Rustemeyer, 2004).

It is essential that gasket materials possess good mechanical performances and sealability. Mechanical performances include compressibility, resilience and stress relaxation property. They are usually used to evaluate abilities to cause gasket material deformation into flange face irregularities under assembly condition, to hold sealing surfaces of joints contacted tightly under internal pressures, and of stress retention at high temperatures, respectively. Sealability is a comprehensive performance of gaskets and indicates the ability to prevent the sealed fluid from leakage through the joints. Sealability can also be called tightness and can be measured quantitatively by the leakage rate.

In the mid 1980s, the American Pressure Vessel Research Committee (PVRC) set up "Room-temperature Mechanical Test Procedure" and "Hot Mechanical Test Procedure" for estimating the probable long-term performance and potential fire survivability of non-asbestos gaskets to guide the qualification and selection of non-asbestos spiral wound, jacketed and sheet gaskets for petroleum and petrochemical plant services in the range of 423-866K. Procedures, test fixtures, and typical test results for several process plant gaskets were discussed. An aged exposure parameter was introduced that correlates cumulative damage with exposure time and temperature for materials that degrade over time (Payne et al., 1989a; Payne et al., 1989b; Payne & Bazergui, 1990). The change in properties of some compressed sheet gasket materials subjected to temperature exposure for periods of up to one year was investigated by Marchand & Derenne. This resulted in a better understanding of the long term effect of thermal degradation on the properties of elastomeric sheet gasket materials. An improved qualification protocol based on the obtainment of the thermal endurance graph of a sheet gasket material was proposed for the extrapolation of the long term service temperature (Marchand & Derenne, 1996). Tsuji et al. researched experimentally the effect of aging time on sealing performance of non-asbestos spiral wound gaskets at elevated temperatures under either the stress controlled condition or the strain controlled condition. The tightness parameter T_p at different elevated temperatures was obtained. The results indicated that the non-asbestos spiral wound gasket had the same sealing performance as the substitute for the asbestos spiral wound gasket between 483 and

693 K (Tsuji et al., 2004). Xie et al. investigated the compressive and resilient performances and relaxation property of the developed compressed non-asbestos fiber reinforced rubber sheet gasket materials, and discussed in detail the effect of the non-asbestos fiber on the properties of the sheet gasket materials (Xie & Cai, 2002; Xie & Xie, 2004).

Systematic researches on gasket performances and their characterizations have been carried out in the Fluid Engineering and Sealing Technology Laboratory at Nanjing University of Technology since the 1980s. The compressive-resilient performance, creep and stress relaxation properties, and leakage behaviour of some types of gaskets were investigated. The representation of gasket performances was put forward, and the formulae for expressing gasket performances were obtained by means of the proposed models and regression analysis of experimental data (Gu et al., 1999; Gu et al., 2000; Gu et al., 2001; Gu, 2002; Zhu et al., 2007; Zhu et al., 2008; Gu et al., 2010). A novel tightness concept was presented, and the tightness analysis and design methods of gasket sealing joints based on the criterion of the maximum allowable leakage rate were developed. Relatively accurate predictions of leakage rates of some gasket sealing connections were also obtained (Gu & Zhu, 1988; Gu & Huang, 1997; Gu et al., 2004; Gu & Chen, 2006; Gu et al., 2007a; Gu et al., 2007b).

Up to now, much work has been fulfilled on the development, performance evaluation and engineering applications of the sealing composites reinforced with non-asbestos fibers, and many results have been achieved. However, relatively comprehensive and systematic reports on design, manufacture and performance evaluation of NASC are still very scarce, especially on the characterization of micro structural parameters, and the mechanical analysis and macro performance prediction of these materials according to the theories of micromechanics and viscoelastic mechanics.

In this chapter, manufacturing technology, surface treatment methods for reinforcing fibers, and formulation design methods of NASC are introduced. Measurements and characterizations of some micro structural parameters of fibers including their aspect ratio, orientation and distribution are investigated. A micromechanical model of single fiber cylindrical cell and a model of compressive type single-fiber cell are established, on the basis of which the methods are proposed for evaluating macro-mechanical performances of NASC, such as tension, compression, and stress relaxation. A leakage model for predicting non-asbestos gasket leakage rates is presented and verified experimentally. Furthermore, the performances of some developed NASC are also evaluated.

2. Manufacturing technology of NASC

2.1 Molding process

The molding process of NASC is similar to that of the traditional rubber based composites, as shown in Fig. 1. The plastication should be carried out using a mill mixer or an internal mixer, to improve plasticity of raw rubber. Before this step, raw rubber may be roasted in a hot chamber within 333-343 K to decrease its hardness and improve manufacturability. The roll temperature of the mill mixer should be controlled below 343 K, and the roller space is about 0.5-1 mm.

The gross rubber is obtained in the mixing step where all accessory ingredients and filling materials are evenly dispersed in broken-down rubber by extrusion and shearing actions of rollers repeatedly.
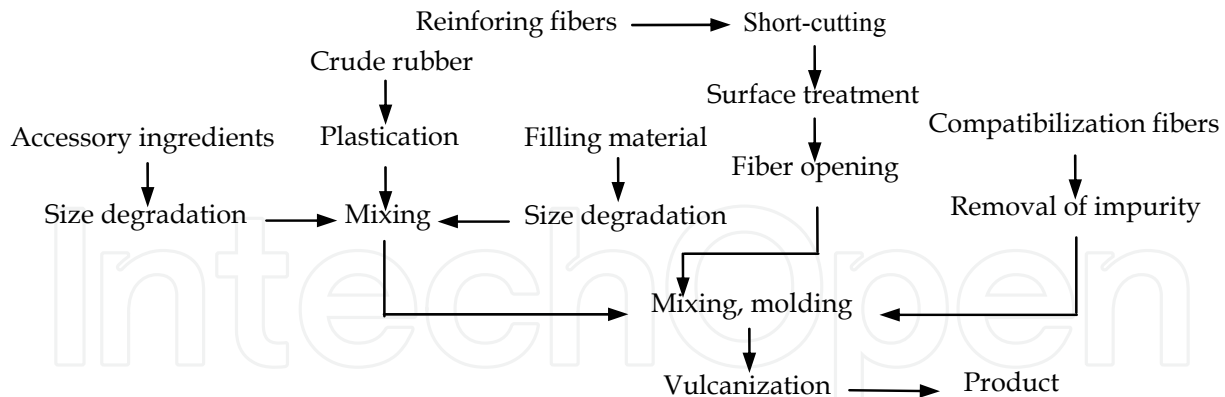
Fig. 1. A molding process of NASC

The mixing step can also be carried out in a mill mixer or an internal mixer. During mixing, the reinforcing fibers can be evenly dispersed in gross rubber, and the aspect ratio of the fibers is reduced to an appropriate value. In the vulcanization step, the rubber and a vulcanizing agent will chemically crosslink at sulfurizing pressures and temperatures. The effect of sulfurization parameters on the transverse tensile strength of aramid fiber reinforced NASC is illustrated in Fig. 2.
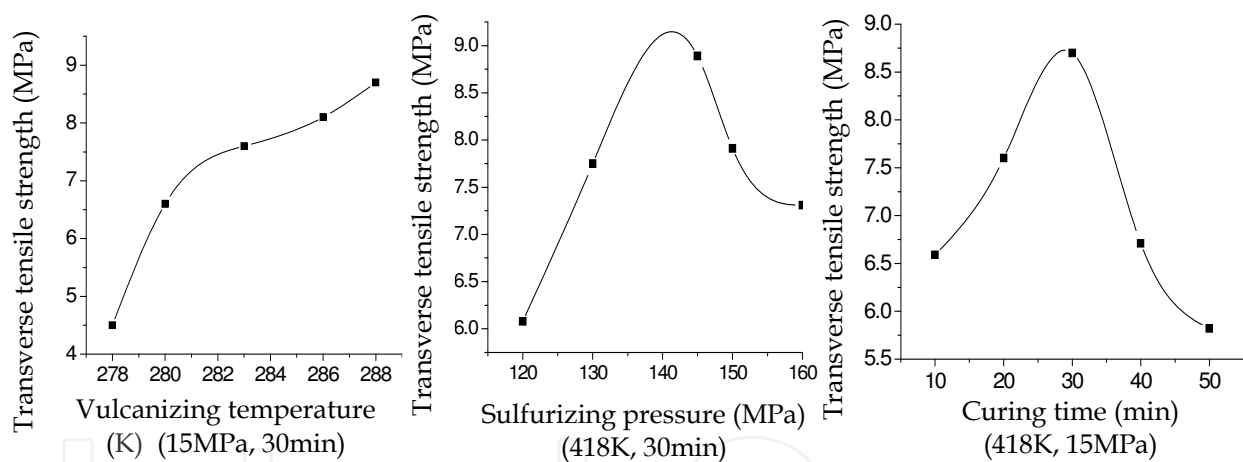

Fig. 2. The effect of sulfurization parameters on transverse tensile strength of aramid fiber reinforced NASC

2.2 Calender process

A calender process flow diagram is illustrated in Fig. 3. In this process, rubber is dissolved by an organic solvent and then mixed with other constituents. The NASC sheet is molded in a roller-type calender.

Preparation of rubber paste is fulfilled in three steps including plasticizing, mixing and dissolving. The mixing and plasticizing steps are the same as those in the molding process. The gross rubber should be separated into small pieces, and then dissolved into the rubber paste by organic solvents, such as gasoline, benzene, methylbenzene and ethyl acetate.

In the mixing step, rubber paste, filling material and reinforcing fibers are mixed, and good quality gross rubber particles with suitable diameter, humidity and hardness are prepared.

Accessory ingredients   Filling material

Rubber → Plastication → Dissolving rubber → Mixing → Calendering

Reinforcing fibers → Surface treatment → Drying → Fiber opening   Vulcanization
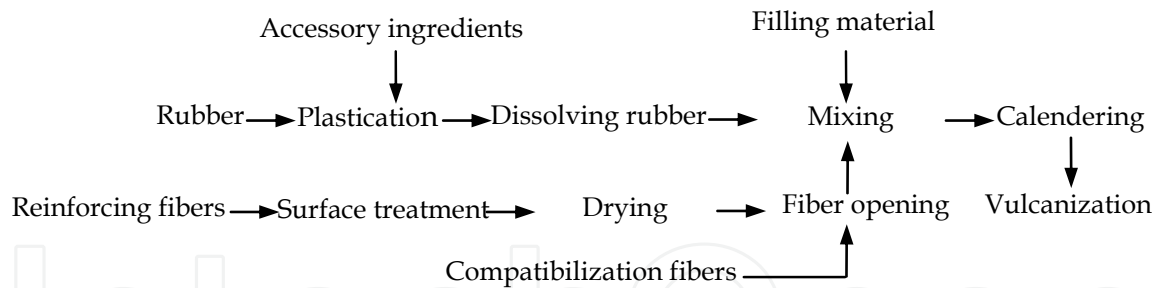
Compatibilization fibers

Fig. 3. A calender process of NASC

The calender process is carried out with two rollers rotating in the opposite directions. Gross rubber particles are fed into the clearance between rollers, and manufactured into NASC sheets. The operating principle of a roller-type calender is shown in Fig. 4.

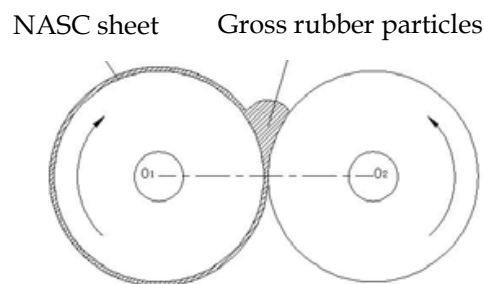NASC sheet   Gross rubber particles

Fig. 4. The operating principle of a roller-type calender

The operating parameters of the calender process mainly include speed ratio of rollers, calender speed (roller surface speed), roller temperature, feed speed, roller clearance and extrusion pressure.

The two rollers are usually thermally stabilized by steam and cool water, respectively. Accordingly, they are called hot roller and cold roller. The appropriate speed ratio of two rollers is in the range of 1.04-1.06.

2.3 Surface treatment of non-asbestos reinforcing short fibers

The surface activity of most non-asbestos fibers is very poor, which leads to the lower wettability between fibers and rubbers. Therefore, in order to obtain a good interface bonding strength, the reinforcing fibers must be pretreated by suitable surface treatment methods. The commonly used surface treatment methods include surface activating treatment and dipping treatment.

Some NASC were developed by the molding process with aramid short fiber as reinforcing fiber, and NBR and NR as elastic binding material. Three surface treatment methods were adopted to pretreat aramid fiber; they are RFL latex dipping, HRH binding agent treatment and silane coupling agent dipping. The results of SEM observation of the developed NASC are shown in Fig. 5.

It can be seen that the surfaces of the aramid fibers without treatment are very smooth, and there are only a few rubber particles adhering on the fiber surfaces. After surface treatments, the adhesion effect between fiber and rubber matrix was obviously improved.

Carbon short fiber can be treated by coupling agent dipping process or epoxide resin coating process after pretreating by air oxidation process or low temperature plasma process. The transverse tensile strength of NASC developed by the calender process was

tested after aging treatment at 623 K, and the results are shown in Fig. 6. It can be seen that surface treatments have improved the reinforcing effects of carbon fiber.

(a) Without surface treatment   (b) Treated by silane coupling

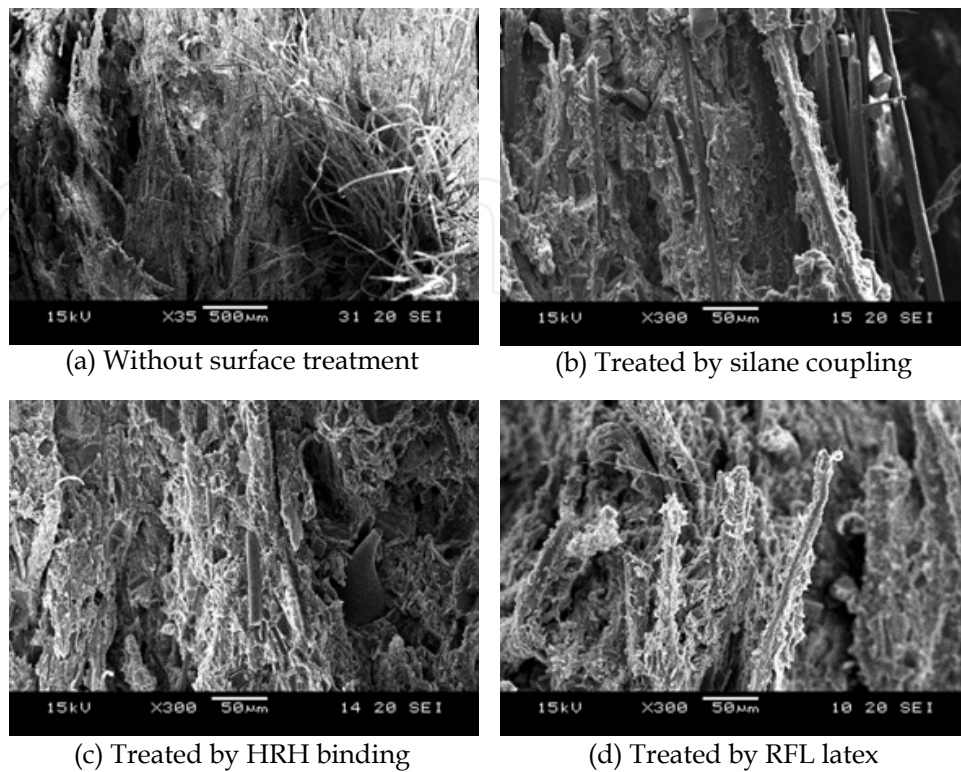(c) Treated by HRH binding   (d) Treated by RFL latex

Fig. 5. SEM photos of transverse tensile fracture sections of aramid fiber reinforced NASC
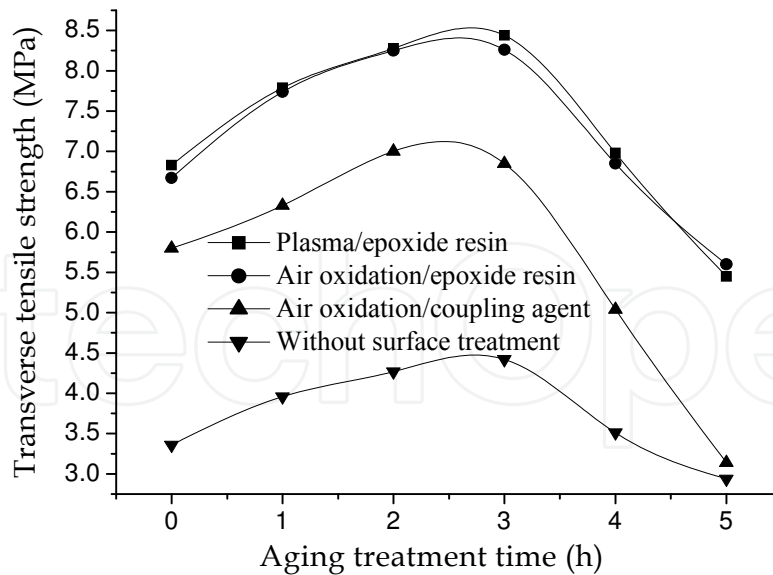

Fig. 6. Transverse tensile strength of carbon fiber reinforced NASC after aging at 623 K

The treatment effect of glass fiber by coupling agent is also distinctive, as illustrated in Fig. 7. The glass fiber should be firstly dipped in a silicon coupling agent water solution for pre-treatment, and then immersed into an epoxide resin methylbenzene solution (2wt%) for further coating treatment. Finally, they must be dried at 423 K to solidify impregnated layer.
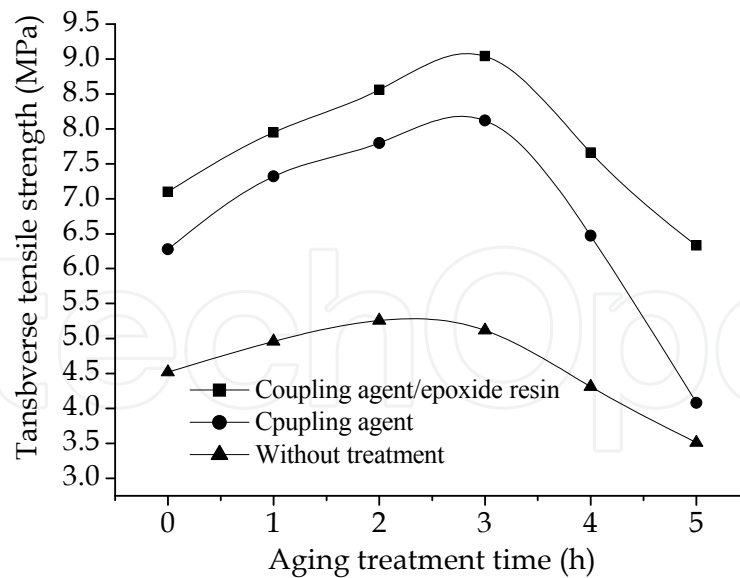
Fig. 7. Transverse tensile strength of glass fiber reinforced NASC after aging at 623 K

The SEM photos of transverse tensile fracture sections of carbon/glass hybrid fiber reinforced NASC aged at 623 K for 5 hours are shown in Fig. 8. It can be seen that the intertwined and the rubber coating conditions of fibres are obviously improved after the surface treatment of the fibers by the coupling agent/epoxide resin coating process.
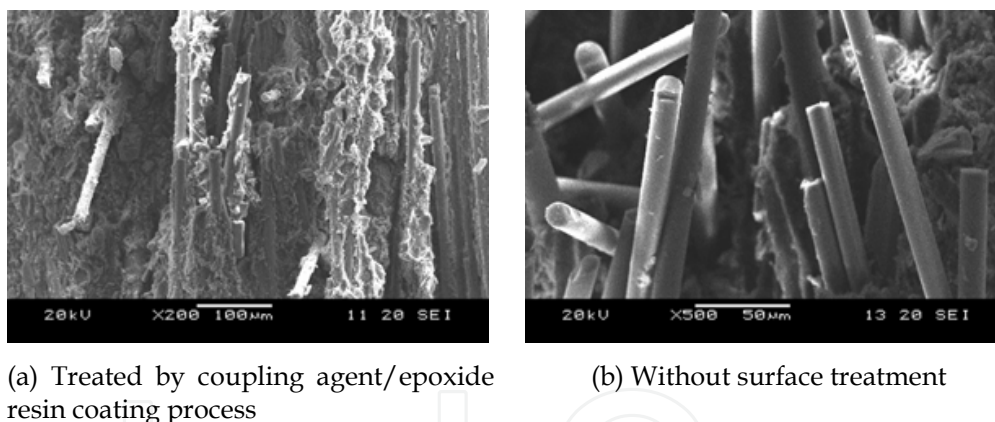

(a) Treated by coupling agent/epoxide resin coating process

(b) Without surface treatment

Fig. 8. SEM photos of transverse tensile fracture sections of carbon/glass hybrid fiber reinforced NASC

3. Formulation design of NASC

3.1 Selection of raw materials for NASC

The main constituents of NASC are non-asbestos reinforcing fibers, elastic binding materials, filling materials and chemical additives. There are great differences of the physicochemical properties between non-asbestos fibers and asbestos fibers. Therefore, in the design of NASC, the effects of the properties and the content of the non-asbestos reinforcing fibers on the performances and manufacturability of the NASC should be paid more attention.

The suitable non-asbestos reinforcing fibers are usually selected according to the performance requirements of NASC. Heat resistance, aspect ratio, medium-resistance, compatibility with rubber, performance-price ratio and source of the reinforcing fibers

should be considered, too. The commonly used non-asbestos reinforcing fibers include carbon fiber, aramid fiber, glass fiber, mineral wool, plant fiber, and so on.

Elastic binding material binds reinforcing fibers and other filling materials together, makes up elastic network structure, and provides compression-resilience and medium-resistance performances of NASC. Natural rubber, nitrile rubber, styrene-butadiene rubber, neoprene rubber, ethylene propylene rubber, fluorine rubber and silicone rubber can all be used as the elastic binding materials of NASC. In consideration of the product performances and price, natural rubber and nitrile rubber are preferably selected.

The filling materials of rubber products include compatibilization filler, reinforcing filler and functional filler. Commonly used filling materials include brucite fiber or sepiolite fiber, carbon black, carbonate, sulphate, metallic oxides, and silicon oxides. In NASC, large grained filler must pair up with short grained filler to maintain proper inter space among rubber bulk material, fibers and filler particles, and ensure sufficient combination between rubber and filler particles.

The selectable accessory ingredients include vulcanizing agents, vulcanization accelerators, vulcanizing activators, anti-aging agents, plasticizing agents and colouring agents etc.. The mixture of dibenzothiazyl disulfide (40 wt%) and tetramethylthiuram disulfide (60 wt%) can be used as a vulcanization accelerator. Zinc oxide (3-5 wt%) and stearic acid (0.5-2 wt%) can be selected as a vulcanizing activator. N-phenyl-n-isopropyl ursol (4010NA) is usually used as the anti-aging agent of rubbers, and the amount is about 1-4wt% (related to rubber weight). Plasticizing agents, colouring agents, solvent, blowing agents, dusting agents and reinforcing resins etc. can also be adopted as accessory ingredients.

3.2 Formulation design of NASC

The uniform design method can be used to further decrease test number in formulation optimization. The approximate formulation of composites can be obtained by uniform design, but the principal and subordinate factors which affect material performances cannot be analyzed by the design table. Furthermore, the regression design can also be adopted to optimize the formulation of NASC. In the mixing regression design, a small quantity of test points will be selected to obtain enough experimental data. According to these data, the regression equation can be derived from the relationship between the test index and the different constituent contents. Finally, the optimization point can be obtained.

3.2.1 Formulation design of aramid fiber reinforced NASC

The formulation design of the aramid fiber reinforced NASC can be defined as the design problem with three components which include reinforcing fiber (aramid fiber), elastic binding material (NBR/NR) and filling material (compatibilization fiber). In consideration of the attribute for processing of the material, the content of components in NASC is limited by Eq. (1).

$$7\% \leq x_1 \leq 22\%, \quad 40\% \leq x_2 \leq 55\%, \quad 10\% \leq x_3 \leq 25\% \tag{1}$$

where x_1, x_2 and x_3 are the weight contents of aramid fiber, compatibilization fiber (brucite fiber or sepiolite fiber) and elastic biding material, respectively.

The contents of other ingredients, such as accessory ingredient, can be determined according to the contents of three components mentioned above. By selecting 5 factor levels for each component, the uniform design scheme for test points is listed in Table 1.

Test points	x_1 (wt%)	x_2 (wt%)	x_3 (wt%)
①	7	43	19
②	10	49	25
③	13	55	17
④	16	40	23
⑤	19	46	15
⑥	22	52	21

Table 1. Experiment scheme according to the uniform design method

According to the test points in Table 1, aramid fiber reinforced materials were developed by the molding process. It can be seen in Table 2 that the transverse tensile strength of the materials developed according to , and test points meets the strength requirement (≥7.0 MPa). The strength of the materials prepared according to and test points are obviously higher than that of scheme . Too much reinforcing fiber in the material of formulation and led to the poor processing manufacturability and low production efficiency, and therefore, formulation was chosen to be the preliminary scheme.

Test points	Transverse tensile strength (MPa)
①	3.55
②	5.26
③	8.81
④	6.75
⑤	10.69
⑥	10.87

Table 2. Transverse tensile strength of aramid fiber reinforced NASC

Results of the single factor experiment about the usage of elastic binding material and aramid fiber are given in Tables 3 and 4, respectively. The aramid fiber and the rubber contents are suggested to be 13 wt% and 20 wt%, respectively.

Performances	Rubber content (wt%)				
	15%	17%	20%	23%	26%
Transverse tensile strength (MPa)	9.22	8.89	8.7	6.87	6.54
Compression rate (%)	4.75	10.06	11.2	13.66	11.4
Resilience rate (%)	43.20	52.15	52.23	51.04	45.7
Stress relaxation rate (%)	28.9	29.4	32.35	37.06	36.15

Table 3. The effect of rubber content on performances of NASC (The amount of aramid fiber is 13 wt%)

Performances	Aramid fiber content (wt%)			
	7%	10%	13%	15%
Transverse tensile strength (MPa)	6.57	7.77	8.70	8.86
Compression rate (%)	15.40	11.36	11.20	9.08
Resilience rate (%)	37.78	48.48	52.23	50.36
Stress relaxation rate (%)	41.42	37.80	32.35	29.42

Table 4. The effect of aramid fiber content on performances of NASC (The amount of elastic binding material is 20 wt%)

The optimization formulation of aramid fiber reinforced NASC is listed in Table 5.

Gradient	Weight content (wt%)	Gradient		Weight content (wt%)
NBR-26	13.0		Calcium carbonate	7.9
NR	7.0	Filling materials	Kaolin clay	3.4
Aramid fiber	13.0		White carbon black	3.4
Compatibilization fiber	45.3		Soap stone powder	2.3
Vulcanizing agent	2.5	Other accessory ingredients		1.8
Curing catalyst	0.4			

Table 5. Formulation of aramid fiber reinforced NASC

3.2.2 Formulation design of carbon/glass hybrid fiber reinforced NASC

The regression design of carbon/glass hybrid fiber reinforced NASC can be defined as the design problem with three components which include reinforcing hybrid fiber (carbon/glass hybrid fiber), elastic binding material (NBR) and filling material (compatibilization fiber and other stuffings). In consideration of the attribute for processing of the material, the component contents in NASC are in the following ranges:

$$0.12 \le X_1 \le 0.25, \ 0.4 \le X_2 \le 0.8, \ 0.1 \le X_3 \le 0.5 \qquad (2)$$

where X_1, X_2 and X_3 are the contents of the elastic binding material, the reinforcing fiber and the filling material, respectively.

The stress relaxation rate y of NASC after ageing treatment at 573 K is used as an evaluating indicator, and the regression design of NASC is to obtain the regression equation by the experiments under the following conditions:

$$a_i \le X_i \le b_i, (i = 1, 2, 3) \quad \text{and} \quad X_1 + X_2 + X_3 = 1 \qquad (3)$$

where a_i and b_i are the constraint conditions described in Eq. (2).

A symmetrical complex Z is established. The coordinate system $x_1 x_2 x_3$ represents the actual design space of the components of NASC, and the coordinate system $z_1 z_2 z_3$ represents the encoding space. Accordingly, the relationship between Z and X can be expressed by:

$$X_1 = a_1 + (b_1 - a_1)z_1/B, \quad X_2 = a_1 + (b_2 - a_2)z_2/B, \quad X_3 = 1 - (X_1 + X_2) \qquad (4)$$

where $B = \max(z_{ij})$, i is the test number, and j the variable number. The coordinates of the actual test points are listed in Table 6, where the stress relaxation rates of the materials after ageing treatment at 573 K are also listed.

The stress relaxation rate of NASC after ageing at 573 K can be expressed by the coordinates of the encoding point, and the regression equation holds:

$$\hat{y} = 63z_1 + 77z_2 + 120.8z_3 - 137.6z_1z_2 + 0.49z_1z_3 - 261.6z_2z_3 \qquad (5)$$

where $\hat{y}$ is the predicted value of the stress relaxation rate of the material, and z_1, z_2 and z_3 are the coordinates of the encoding point.

NO.	Encoding content of components			Actual content of components			Relaxation rate y (%)
	z_1	z_2	z_3	X_1	X_2	X_3	
1	0	1/2	1/2	0.12	0.667	0.213	51.6
2	1/2	0	1/2	0.207	0.4	0.393	32.9
3	1/2	1/2	0	0.207	0.667	0.127	43.9
4	1/4	1/4	1/2	0.163	0.533	0.303	34.6
5	1/4	1/2	1/4	0.163	0.667	0.17	42.3
6	1/2	1/4	1/4	0.207	0.533	0.26	31.3
7	3/4	1/8	1/8	0.25	0.467	0.283	58.4
8	1/8	3/4	1/8	0.142	0.8	0.058	52.4
9	1/8	1/8	3/4	0.142	0.467	0.392	43.1

Table 6. Experimental scheme and test results

The purpose of prescription optimization is to improve the heat resistance and the attribute for processing of NASC, to reduce the self-cost of the raw materials of the product, and to ensure the stress relaxation rate of the material satisfying the index prescribed in the product standard. The prescription optimization of NASC is to obtain the optimal values of z_1, z_2 and z_3 under the following conditions:

$$z_i \geq 0, \ \sum_{i=1}^{3} z_i = 1, \ z_1 = z_{1min}, \ z_2 = z_{2min}, \hat{y} \leq 35 \ (i = 1,2,3) \tag{6}$$

According to Eq. (5), the coordinates of the best theoretic design point of the contents of the components in NASC can be obtained, as z_1=0.38, z_2=0 and z_3=0.63. From Eq. (4), the formulation is x_1=0.186, x_2=0.4 and x_3=0.414.

Some NASC were prepared when the weight ratio (carbon fiber to glass fiber) equalled to 4:0, 3:1, 2:2, 1:2, 1:3 and 0:4 respectively. The experimental results of the transverse tensile strength and the stress relaxation rate of these materials after ageing treatment at 573 K for 5 hours are shown in Fig. 9. It can be found that the strength of the material is the highest and the relaxation rate is relatively low when the weight ratio is 2:3 (weight content of carbon fiber in hybrid fibers is 40%).
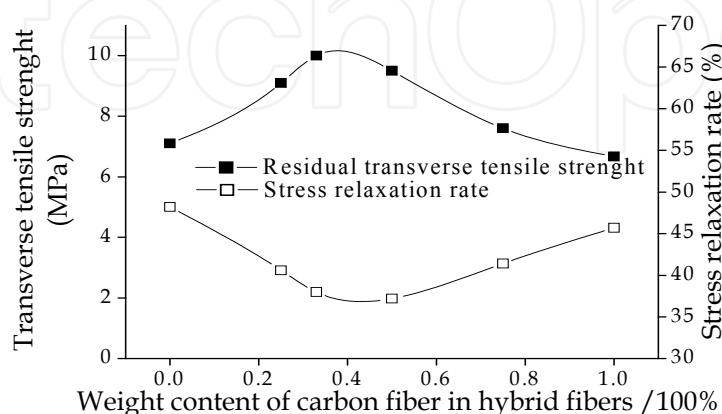

Fig. 9. The effect of carbon fiber content in hybrid fibers on transverse tensile strength and stress relaxation rate of NAFC

Therefore, the optimization formulation of the NASC reinforced with carbon/glass hybrid fibers was obtained, as listed in Table 7.

Component	Content (wt%)	Component		Content (wt%)
NBR	18.6	Accelerating agent		0.22
Carbon fiber	16.0	Zinc white		0.48
Glass fiber	24.0	Stearinic acid		0.18
Sepiolite fiber	10.3	Antiaging protective		0.6
Phenolic resin	8.38	Filling material	Lime carbonate	6.31
Hyperfine graphite powder	7.44		Kaolin clay	3.2
Vulcanized agent	0.35		Soap stone powder	1.6
			Carbon black	2.34

Table 7. Formulation of carbon/glass hybrid fibers reinforced NASC

4. Measurement and characterization of micro structures of NASC

4.1 Measurement and characterization of aspect ratio

The aspect ratio of short fiber determines the transfer and distribution of stress in material, and its distribution regularity can be obtained by measuring the radius and the length of fibers in the NASC products. Some samples of NASC were prepared. Using organic solvents, such as gasoline or toluene, to dissolve the matrix rubber, the short fibers different in size are left and dried. Considering the fiber radius is about micron, a digital camera with high-resolution is used to take pictures of fibers, and the length and radius of each short fiber are obtained by numerically analyzing the pictures. Then the distribution of aspect ratios can be obtained by counting the aspect ratios of 500 to 1000 fibers. The typical histograms of aspect ratios of aramid fibers can be seen in Fig. 10.
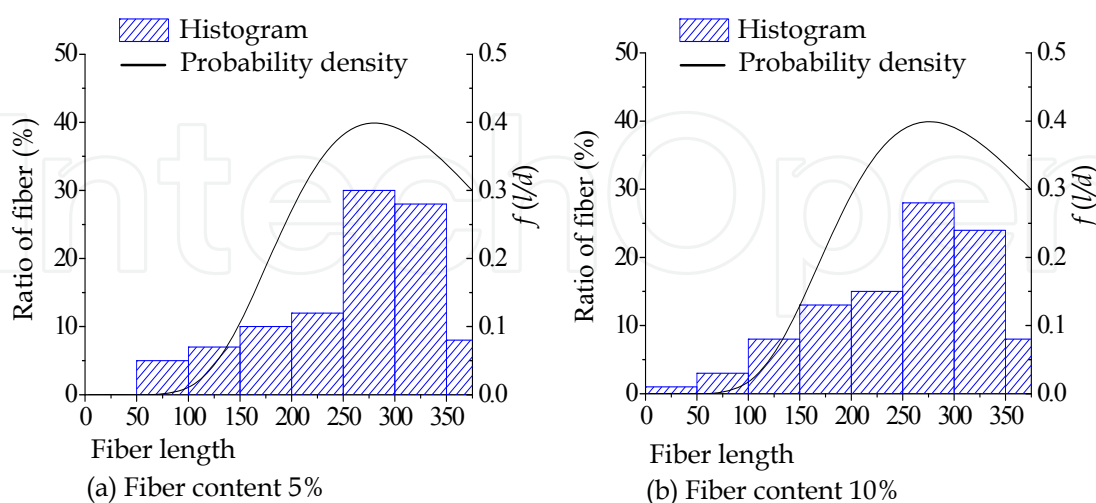

Fig. 10. Aspect ratio distribution of aramid fibers with the initial length of 4-6 mm

The distribution of aspect ratios in NASC is influenced by the initial aspect ratio, the rapture characteristic and the content of fibers, the matrix characteristic and the preparation process.

If the aspect ratio varies in a relatively small range, it can be characterized by the mean aspect ratio. If it distributes dispersedly, however, the characterization with a distribution function is appropriate. Furthermore, a histogram can also be used to express the distribution of aspect ratios without considering the dispersity of aspect ratios.

The log-normal density function is usually used to characterize the aspect ratios, as Eq. (7) expresses.

$$f(l/d) = \frac{1}{\sqrt{2\pi}} \exp\left[-\frac{\left[\ln(l/d) - a\right]^2}{2b^2}\right] \tag{7}$$

where $a = \sqrt{2\left[\ln(\bar{l}/d) - \ln(l_{mod}/d)\right]/3}$, $b = \left[2\ln(\bar{l}/d) + \ln(l_{mod}/d)\right]/3$, $\bar{l}/d$ is the mean aspect ratio and l_{mod}/d the maximum probability density of the aspect ratio.

The arithmetical mean of aspect ratios can be calculated by Eq. (8).

$$\bar{l_s}/d = \frac{1}{m}\sum_{n=1}^{m}(l_n/d) \tag{8}$$

where $\bar{l_s}/d$ is the average value of aspect ratios, m is the number of short fibers and l_n/d is the aspect ratio of the number n short fiber. The arithmetical mean aspect ratio can also be calculated by Eq. (9) if the histogram of aspect ratios is known.

$$\bar{l_s}/d = \sum p_i(l_i/d)/\sum p_i \tag{9}$$

where l_i/d is the aspect ratio of fibers in the interval i, and p_i is the ratio of the number of fibers whose aspect ratios are in the interval i to the total number of fibers.

4.2 Measurement and characterization of fiber orientation

Investigating the orientation of fibers in matrix will provide both theoretical explanations for the reinforcing mechanism of short fibers and the basis for prediction and optimization of mechanical properties of NASC.
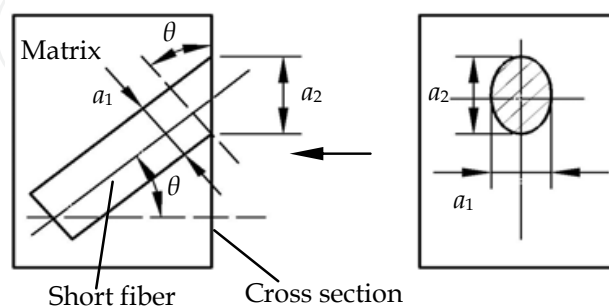

Fig. 11. A schematic diagram of the section-analysis method

A proprietary technology was developed to obtain the fiber orientation in matrix. Four steps are involved. Firstly, cut a rectangular block of material and hold it in position by a clamp in the slicer. Secondly, slice the cross section of the material block at -423 K using the slicer

knife to machine a smooth end face, of which the normal direction should be along the rolling direction. Thirdly, visually observe the end face using a microscope associated with a high-resolution digital camera. Finally, analyze the photos and find out the configuration of the elliptical cross section of fibers. The orientation angle can be determined from the long axis and the short axis of the ellipse, as illustrated in Fig. 11.

The normal direction of the cross section is in accordance with the reference direction, and the orientation angle θ is the separation angle between the axial direction of a fiber and the reference direction. The relationship among θ and the long axis length a_1 and the short axis length a_2 is in the form

$$\theta = \arccos\left(a_1/a_2\right) \tag{10}$$

The orientation of a fiber can be characterized by a histogram, a distribution function or modified coefficients. The orientation expressed by an exponential density function $f(\theta)$ is

$$f\left(\theta\right) = \xi\exp\left(-\lambda\theta\right)/1 - \exp\left(-\pi\lambda/2\right) \tag{11}$$

where ξ is the fiber orientation parameter. In order to utilize the results of the fiber orientation characterization to predict the macro mechanical properties of NASC, the modified coefficients are introduced. The longitudinal modified coefficient $f_{\theta1}$ can be calculated by Eq. (12) based on the distribution function.

$$f_{\theta1} = \int_0^{\frac{\pi}{2}} f\left(\theta\right)\cos^2\theta\mathrm{d}\theta \tag{12}$$

$f_{\theta1}$ is employed to evaluate the influence of fiber orientations on longitudinal mechanical property. The transversal mechanical property is evaluated by the transverse orientation coefficient $f_{\theta2}$ which can also be obtained based on a distribution function or a histogram given by Eqs. (13) and (14), respectively.

$$f_{\theta2} = \int_0^{\frac{\pi}{2}} f\left(\theta\right)\sin\theta\cos\theta\mathrm{d}\theta \tag{13}$$

$$f_{\theta2} = \sum_{n=1}^{m_\theta} f_\theta\left(\theta_n\right)\sin\theta_n\cos\theta_n \tag{14}$$

4.3 Fiber distribution in matrix

Theoretical work on NASC is usually based on the assumption that fibers are stiff and straight in matrix. The real fibers, however, bend and wind together. With the reduce of fiber contents or the increase of fiber lengths, fiber bending and winding are enhanced. Due to the forming process, the bending, winding and uneven distribution of fibers always exist randomly and are very difficult to be characterized.

4.4 Thickness of interface

For most fiber reinforced composites, the thickness of interface between a fiber and the matrix is very small and hence is usually not considered. For NASC, however, to enhance

the reinforcing effect of fibers and to optimize the bonding capability of fiber surface, short fibers should be pretreated using surface conditioning agents before mixing, and the interface has great influence on mechanical properties of NASC. The interface thickness can be easily determined by calculating the change in the fiber radius before and after pretreatment.

4.5 Porosity

Some pores will occur during the preparation process of NASC, especially in the sulfuration process. Most of these pores exist in the interface and they will change the stress transfer mode. The porosity p, which is the ratio of the total volume of all pores to the volume of the composite, can be used to evaluate the volume fraction of pores in the composite.

5. A micromechanical model and prediction of macro performances

Loads exerting on NASC will be transferred to fibers through matrix, and the mechanism relates to constitutive equations and mechanical behaviors of fibers, matrix and interface phase. According to the thermo-viscoelastic theory and the shear-lag theory of fibrous composites, a micromechanical model of a single fiber cylindrical cell, which includes a fiber, the matrix and their interphase, is established.

5.1 A micromechanical model of NASC

Fig. 12 illustrates a micromechanical model of NASC, where l is the fiber length, L the matrix length and $L \approx l$. The volume content of fiber is V_f.
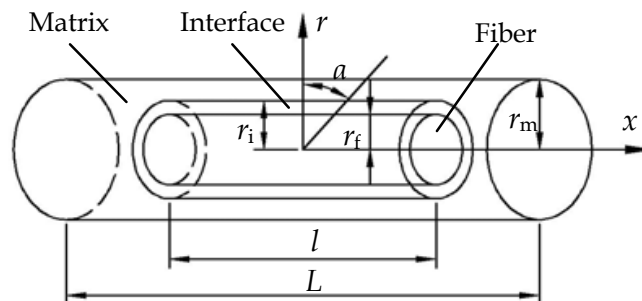

Fig. 12. A micromechanical model of NASC

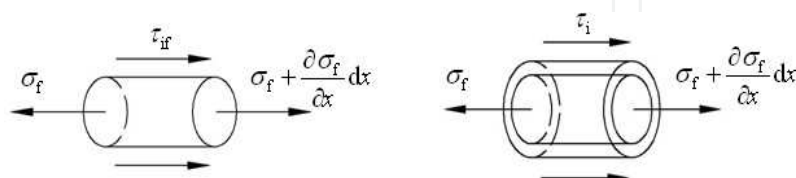The stress transfer procedure can be seen in Fig. 13.

Fig. 13. Micromechanical stress transfer in NASC

When the single fiber cylindrical cell is only subjected to the tension load along the x axis, the circumferential and the radial stresses in the model are much less than the axial stress, and they can be neglected.

The equilibrium relationship of the stresses shown in Fig. 13 can be expressed by

$$\frac{\partial \sigma_f(x)}{\partial x} = -\frac{2\tau_{if}(x)}{r_f} \tag{15}$$

where $\sigma(x)$ is the axial stress in fiber and $\tau_{if}(x)$ is the shear stress on fiber surface. The axial shear stress in matrix $\tau_m(r, x)$ can be expressed by

$$\tau_m(r,x) = \frac{(r_m^2 - r^2)r_i}{(r_m^2 - r_i^2)r}\tau_{im}(x) \tag{16}$$

where $\tau_{im}(x)$ is the shear stress at the interface boundary near the matrix.

The shear stress in the matrix is a time dependent physical quantity, and it holds the following relationship with the shear strain.

$$\frac{\partial u_m(r,x,t)}{\partial r} = \int_{0^-}^{t} J_{\tau m}(t-s)d\tau_m(r,x,t) \tag{17}$$

where $u_m(r, x, t)$ is the axial displacements of the matrix, and $J_{\tau m}(t-s)$ is the creep function. If the bond of both the matrix and the fiber with interface ideally, the axial displacement of the matrix can be expressed by

$$u_m(r,x,t) = u_i(r_f,x,t) + \frac{r_f}{\mu_i}\ln\left(\frac{r_i}{r_f}\right)\tau_{if}(x,t) + \frac{\left[2r_m^2\ln(r/r_i) - (r^2 - r_i^2)\right]r_i}{2(r_m^2 - r_i^2)}\int_{0^-}^{t} J_{\tau m}(t-s)d\tau_{im}(x,t) \tag{18}$$

The strain of the matrix $\varepsilon_m(r, x, t)$ holds

$$\varepsilon_m(r,x,t) = \frac{\partial u_m(r,x,t)}{\partial x} = \frac{\sigma_f(x)}{E_f} + \alpha_f \Delta T - \frac{r_f^2}{2\mu_i}\ln\left(\frac{r_i}{r_f}\right)\frac{\partial^2 \sigma_f(x,0)}{\partial x^2}$$

$$-\frac{\left[2r_m^2\ln(r/r_i) - (r^2 - r_i^2)\right]r_f^2}{4(r_m^2 - r_i^2)}\left[J_{\tau m}(t)\frac{\partial^2 \sigma_f(x,0)}{\partial x^2} - \int_{0^+}^{t} J_{\tau m}(t-s)\frac{\partial^2 \dot{\sigma}_f(x,s)}{\partial x^2}ds\right] \tag{19}$$

According to the viscoelastic theory, the shear stress of the matrix $\tau_{if}(x, t)$ holds

$$\tau_{if}(x,t) = \frac{u_m(r_m,x,t) - u_i(r_f,x,t) - \frac{r_f}{\mu_i}\ln\left(\frac{r_i}{r_f}\right)\tau_{if}(x,t)}{\left[2r_m^2\ln(r_m/r_i) - (r_m^2 - r_i^2)\right]r_f / \left[2(r_m^2 - r_i^2)\right]}dG_{\tau m} \tag{20}$$

where $G_{\tau m}$ is the relaxation function of $\tau_{if}(x, t)$. Differentiating $\sigma_f(x, t)$ by x gives

$$\frac{\partial^2 \sigma_f(x,t)}{\partial x^2} = -\frac{2\left[\frac{\partial u_m(r_m,x,t)}{\partial x} - \frac{\partial u_i(r_f,x,t)}{\partial x} + \frac{r_f^2}{2\mu_i}\ln\left(\frac{r_i}{r_f}\right)\frac{\partial^2 \sigma_f(x,t)}{\partial x^2}\right]}{\left[2r_m^2\ln(r_m/r_i) - (r_m^2 - r_i^2)\right]r_f^2 / \left[2(r_m^2 - r_i^2)\right]}dG_{\tau m} \tag{21}$$

Considering $u_i(r_f, x, t) = u_f(r_f, x, t)$, $\dfrac{\partial u_i(r_f, x, t)}{\partial x} = \dfrac{\partial u_f(r_f, x, t)}{\partial x} = \varepsilon_f = \dfrac{\sigma_f(x,t)}{E_f} + a_f \Delta T$ and

$\dfrac{\partial u_m(r_m, x, t)}{\partial x} = \varepsilon_m(r_m, t)$, Eq. (22) is obtained.

$$\frac{\partial^2 \sigma_f(x,t)}{\partial x^2} + \frac{2\dfrac{r_f^2}{2\mu_i} ln\left(\dfrac{r_i}{r_f}\right)}{\left[2r_m^2 ln(r_m/r_i) - (r_m^2 - r_i^2)\right] r_f^2 \Big/ \left[2(r_m^2 - r_i^2)\right]} \left[\frac{\partial^2 \sigma_f(x,t)}{\partial x^2} G_{tm}(0) + \int_{0^+}^{t} \frac{\partial^2 \sigma_f(x,s)}{\partial x^2} \dot{G}_{tm}(t-s) ds\right]$$

$$- \frac{2}{\left[2r_m^2 ln(r_m/r_i) - (r_m^2 - r_i^2)\right] r_f^2 E_f \Big/ \left[2(r_m^2 - r_i^2)\right]} \left[\sigma_f(x,t) G_{tm}(0) + \int_{0^+}^{t} \sigma_f(x,s) \dot{G}_{tm}(t-s) ds\right] \quad (22)$$

$$+ \frac{2\left[\varepsilon_m(r_m, t) - a_f \Delta T\right]}{\left[2r_m^2 ln(r_m/r_i) - (r_m^2 - r_i^2)\right] r_f^2 \Big/ \left[2(r_m^2 - r_i^2)\right]} dG_{tm} = 0$$

Eq. (22) is the micromechanical model of NASC which expresses the stress transfer regularity among the matrix, the fiber and their interface.

(a) Axial stress distribution in fibers   (b) Axial stress distribution in interface
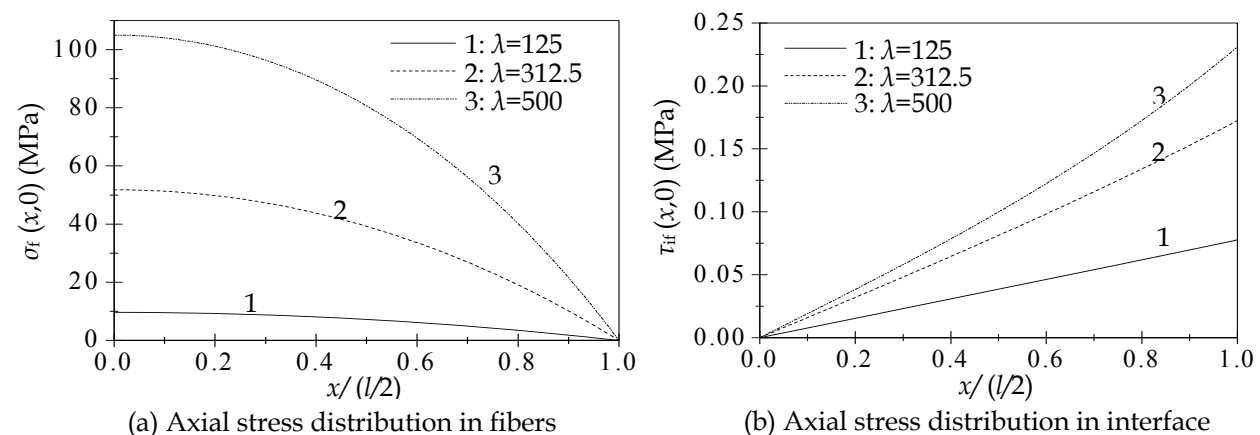
Fig. 14. Influence of the fiber aspect ratio on the stress distribution

The stresses in fibers and interface are illustrated in Fig. 14, where the coordinate x represents the axial distance from the midst ($x=0$) to the end ($x=l/2$) of the fibers. Fig. 14(a) reveals that the axial stress in the fibers σ_f reduces from the midst to the end, and with the increasing aspect ratio λ, σ_f at the fiber end increases. Fig. 14(b) illustrates the shear stress distribution in interface at the fiber side, and the shear stress increases from the midst to the end.

5.2 Prediction of mechanical performances of NASC
5.2.1 Prediction of the stress-strain relationship
Since the module of interface is much smaller than that of fibers and the interface thickness is much smaller than the matrix, the load is borne mainly by the fibers and the matrix. When the aspect ratio of the fiber is no larger than a critical value, the stress-strain relationship can be expressed by

$$\sigma_c(\varepsilon_c) = f_{\theta 1} f_i f_f V_f \overline{\sigma}_f(\varepsilon_c) + V_m \overline{\sigma}_m(\varepsilon_c) \quad (23)$$

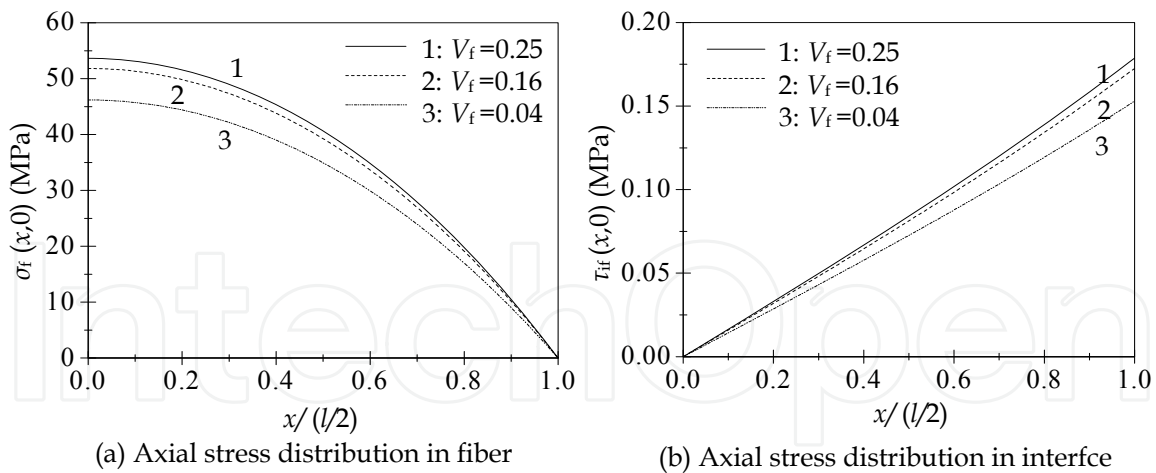(a) Axial stress distribution in fiber   (b) Axial stress distribution in interfce

Fig. 15. Influence of the fiber volume fraction on the stress distribution

where $f_{\theta 1}=1$ when all fibers are parallel to the load direction, otherwise $f_{\theta 1}=0.5$; f_i is the correction coefficient for interface performance obtained by experiments; $f_f=\left(1-V_f^2\right)$ and

$$\bar{\sigma}_f\left(\varepsilon_C\right)=\left[1-\frac{\tanh\left(\beta_0\lambda/a_0\right)}{\beta_0\lambda/a_0}\right]E_f\left(\varepsilon_c-a_f\Delta T\right),\quad\bar{\sigma}_m(\varepsilon_c)=E_m\varepsilon_c \tag{24}$$

When the aspect ratio of the fibers is larger than the critical value, the relationship between stress and strain can be expressed by

$$\sigma_c\left(\varepsilon_c\right)=\begin{cases}f_{\theta 1}f_if_fV_f\bar{\sigma}_f\left(\varepsilon_c,\bar{\lambda}\right)+V_m\bar{\sigma}_m\left(\varepsilon_c,\bar{\lambda}\right) & \varepsilon_c\le\varepsilon_{cf}\\ f_{\theta 1}f_if_fV_f\bar{\sigma}_f\left(\varepsilon_c,\bar{\lambda}/2\right)+V_m\bar{\sigma}_m\left(\varepsilon_c,\bar{\lambda}/2\right) & \varepsilon_c>\varepsilon_{cf}\end{cases} \tag{25}$$

where ε_{cf} is the tensile strain of the fibers at the time it breaks, which holds

$$\varepsilon_{cf}=\sigma_{fu}^T\left/\left\{E_f\left[1-\frac{1}{\cosh\left(\beta_0\lambda/a_0\right)}\right]\right\}\right.+a_f\Delta T \tag{26}$$

5.2.2 Prediction of the tensile module

Due to the effect of fibers, the maximum permissible deformation of NASC is only about 10% of that of rubber and the bearing capacity of NASC is greatly improved. The tensile module can be used to characterize the bearing capacity of NASC. The longitudinal tensile module E_{cL} can be calculated by Eq. (27) if the aspect ratios of fibers are relatively concentrated, otherwise it can be calculated by Eq. (28).

$$E_{cL}=f_p\left(f_{\theta 1}f_if_fV_f\frac{\bar{\sigma}_f}{\varepsilon_c}+V_mE_m\right) \tag{27}$$

$$E_{cL}=f_p\left(\sum_{n=1}^m f_{\theta 1}f_if_fV_{fn}\frac{\bar{\sigma}_{fn}}{\varepsilon_c}+f_mV_mE_m\right) \tag{28}$$

where $\overline{\sigma}_{\mathrm{fn}}$ can be calculated according to Eq. (29).

$$\overline{\sigma}_{\mathrm{fn}} = \left[1 - \frac{\tanh\left(\beta_0 \overline{\lambda}_{\mathrm{n}}/\alpha_0\right)}{\beta_0 \lambda/\alpha_0} \right] E_{\mathrm{f}} \left(\varepsilon_{\mathrm{c}} - \alpha_{\mathrm{f}} \Delta T\right) \tag{29}$$

where $\overline{\lambda}_{\mathrm{n}}$ is the mean aspect ratio of fibers with the length l_{n}, V_{fn} is the volume content of fibers with the length l_{n}, and $f_{\mathrm{p}} = 1 - 1.9p + 0.9p^2$. The Halpin-Tsai equation is employed to predict the transverse tensile module of NASC E_{cH} with single orientation.

$$E_{\mathrm{cH}} = \frac{1 + 2\eta V_{\mathrm{f}}}{1 - \eta V_{\mathrm{f}}} E_{\mathrm{m}} \tag{30}$$

where

$$\eta = \frac{E_{\mathrm{f}}/E_{\mathrm{m}} - 1}{E_{\mathrm{f}}/E_{\mathrm{m}} + 2} \tag{31}$$

In consideration of the effect of fiber length and orientation and porosity of material on the transverse tensile module, Eq. (32) is established.

$$E_{\mathrm{cH}} = f_{\mathrm{p}} \left(\frac{1 + 2V_{\mathrm{f}}}{1 - V_{\mathrm{f}}} E_{\mathrm{m}} + f_{\theta 2} f_{\mathrm{i}} f_{\mathrm{f}} V_{\mathrm{f}} \frac{\overline{\sigma}_{\mathrm{f}}}{\varepsilon_{\mathrm{c}}} \right) \tag{32}$$

5.2.3 Prediction of the longitudinal tensile strength

The temperature-related longitudinal tensile strength σ_{cL}^T of NASC can be calculated by Eq. (33).

$$\sigma_{\mathrm{cL}}^T = f_{\theta 1} f_{\mathrm{i}} f_{\mathrm{f}} V_{\mathrm{f}} \overline{\sigma_{\mathrm{f}}^T} + f_{\mathrm{d}} V_{\mathrm{m}} \overline{\sigma_{\mathrm{m}}^T} \tag{33}$$

where $f_{\mathrm{d}} = \left(1 - V_{\mathrm{f}}\right)$, $\overline{\sigma_{\mathrm{f}}^T}$ is the mean stress in fibers when tensile failure occurs and it can be obtained from the micromechanical model of NASC, $\overline{\sigma_{\mathrm{m}}^T}$ is the mean stress in the matrix when tensile failure occurs and $\overline{\sigma_{\mathrm{m}}^T} = E_{\mathrm{m}}^T \varepsilon_{\mathrm{cu}}^T$, and f_{d} is the weakening coefficient of rubber induced by fibers.

When the aspect ratio λ is smaller than the critical value λ_{c}, the debonding between fibers and the matrix will occur. However, when $\lambda > \lambda_{\mathrm{c}}$, the fiber breaks. Therefore, the temperature-related longitudinal tensile strength can be calculated according to Eq. (34).

$$\sigma_{\mathrm{cL}}^T = f_{\theta 1} f_{\mathrm{i}} f_{\mathrm{f}} V_{\mathrm{f}} \left[\int_{\lambda_{\min}}^{\lambda_{\mathrm{c}}} f(\lambda) \lambda \left(\tau_{\mathrm{s}}^T - \Delta\tau_{\mathrm{i}}^T\right) \mathrm{d}\lambda + \int_{\lambda_{\mathrm{c}}}^{\lambda_{\max}} f(\lambda)\left(1 - 0.5\lambda_{\mathrm{c}}/\lambda\right)\left(\sigma_{\mathrm{fu}}^T - \Delta\sigma_{\mathrm{f}}^T\right) \mathrm{d}l \right] + f_{\mathrm{d}} V_{\mathrm{m}} \overline{\sigma_{\mathrm{mm}}^T} \tag{34}$$

where $\Delta\sigma_{\mathrm{f}}^T$ is the stress in fibers induced by temperature change and $\Delta\tau_{\mathrm{i}}^T$ is the shear stress in fibers, $\Delta\sigma_{\mathrm{f}}^T = \left[1 - \frac{\tanh\left(\beta_0 \lambda/\alpha_0\right)}{\beta_0 \lambda/\alpha_0} \right] E_{\mathrm{f}} \alpha_{\mathrm{f}} \Delta T$ and $\Delta\tau_{\mathrm{i}}^T = \frac{E_{\mathrm{f}} \alpha_{\mathrm{f}} \Delta T}{\lambda}$.

5.2.4 Prediction of the transverse tensile strength

The transverse tensile strength is a main evaluating indicator for NASC in engineering, and its prediction may be performed according to 3 cases, as follows.

1. Debonding of interface from fiber

In this case, the transverse tensile strength σ_{cH}^{T} can be calculated by

$$\sigma_{cH}^{T} = \sqrt{\pi V_f}\tau_{if}^{T} + 2\frac{t_i}{r_f}\sqrt{\frac{V_f}{\pi}}\sigma_{iH}^{T} + \left(1 - 2\frac{t_i + r_f}{r_f}\sqrt{\frac{V_f}{\pi}}\right)\sigma_{mH}^{T} \tag{35}$$

Eq. (35) can be used to predict the transverse tensile strength assuming that all fibers orientate in the same direction at the moment the matrix debonds from the fibers. If the fibers orientate in different directions, some will bear the longitudinal load. In this case, the transverse tensile strength is larger than that calculated by Eq. (35), and it can be calculated by Eq. (36).

$$\sigma_{cH}^{T} = f_{\theta3}\left(\sqrt{V_f\pi}\tau_{if}^{T} + 2\frac{t_i}{r_f}\sqrt{\frac{V_f}{\pi}}\sigma_{iH}^{T}\right) + f_{\theta2}f_i f_f V_f \overline{\sigma_f^{T}} + \left(1 - 2\frac{t_i + r_f}{r_f}\sqrt{\frac{V_f}{\pi}}\right)\sigma_{mH}^{T} \tag{36}$$

2. Debonding of interface from matrix

If all fibers orientate in the same direction at the moment the interface debonds from the matrix, the transverse tensile strength σ_{cH}^{T} can be calculated by Eq. (37).

$$\sigma_{cH}^{T} = \frac{t_i + r_f}{r_f}\sqrt{V_f\pi}\tau_{im}^{T} + \left(1 - 2\frac{t_i + r_f}{r_f}\sqrt{\frac{V_f}{\pi}}\right)\sigma_{mH}^{T} \tag{37}$$

If fibers orientate in different directions, σ_{cH}^{T} can be calculated by Eq. (38).

$$\sigma_{cH}^{T} = f_{\theta3}\frac{t_i + r_f}{r_f}\sqrt{\pi V_f}\tau_{im}^{T} + f_{\theta2}f_i f_f V_f \overline{\sigma_f^{T}} + \left(1 - 2\frac{t_i + r_f}{r_f}\sqrt{\frac{V_f}{\pi}}\right)\sigma_{mH}^{T} \tag{38}$$

3. Damage of interface

The transverse tensile strength can be calculated by

$$\sigma_{cH}^{T} = \frac{F_H}{WL} = \sqrt{V_f\pi}\tau_{is}^{T} + 2\frac{t_i}{r_f}\sqrt{\frac{V_f}{\pi}}\sigma_{iH}^{T} + \left(1 - 2\frac{t_i + r_f}{r_f}\sqrt{\frac{V_f}{\pi}}\right)\sigma_{mH}^{T} \tag{39}$$

Using Eq. (39), the transverse tensile strength σ_{cH}^{T} can be predicted assuming that all fibers orientate in the same direction at the moment the interface is damaged. If fibers orientate in different directions, σ_{cH}^{T} can be calculated by Eq. (40).

$$\sigma_{cH}^{T} = f_{\theta3}\left(\sqrt{V_f\pi}\tau_{is}^{T} + 2\frac{t_i}{r_f}\sqrt{\frac{V_f}{\pi}}\sigma_{iH}^{T}\right) + f_{\theta2}f_i f_f V_f \overline{\sigma_f^{T}} + \left(1 - 2\frac{t_i + r_f}{r_f}\sqrt{\frac{V_f}{\pi}}\right)\sigma_{mH}^{T} \tag{40}$$

5.2.5 Prediction of compression-resilience performances

NASC is used to make gaskets, and the direction of compressive loads acting on it is normal to the orientation direction of fibers. The model of a compressive type single-fiber cell (Fig.

16) is established to derive the compression-creep constitutive equation of NASC with the assumption $L \approx l$. The cell model is divided into three parts along compression-resilience direction; the first part consists of matrix, interface and fiber (0-1), the second part consists of matrix and interface (1-2), and the third part includes only matrix (2-3).
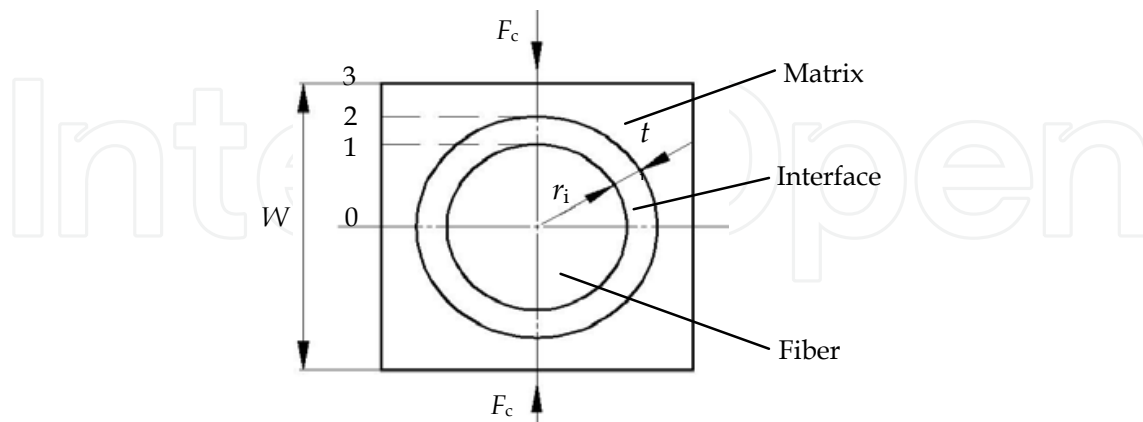

Fig. 16. A model of a compressive type single-fiber cell

The total strain of the material ε_{cc} under the load F_c holds

$$\varepsilon_{cc} = \frac{2}{W}\left[\varepsilon_{c0\text{-}1}r_f + \varepsilon_{c1\text{-}2}t_i + \varepsilon_{c2\text{-}3}\left(\frac{W}{2} - t_i - r_f\right)\right] \tag{41}$$

The compressive stress and strain of material relate to time. The compression-creep constitutive equation of NASC is in the form

$$\varepsilon_{cc}(t) = \left(\frac{2}{\sqrt{2}E_f} + \frac{2t_i}{\sqrt{t_i^2 + 2t_i r_f}\,E_i}\right)\sigma_{cc}(t) + 2\left[\sigma_{cc}(0)J_{cm}^T(t) + \int_{0^+}^{t} J_{cm}^T(t-\varsigma)\frac{d\sigma_{cc}(\varsigma)}{d\varsigma}d\varsigma\right]$$
$$\times\left(\frac{1}{2} - \frac{t_i\sqrt{V_f/\pi}}{r_f} - \sqrt{V_f/\pi}\right) - \left[2\alpha_f\sqrt{V_f/\pi} + \frac{2\alpha_i t_i}{r_f}\sqrt{V_f/\pi} + 2\alpha_m\left(\frac{1}{2} - \frac{t_i\sqrt{V_f/\pi}}{r_f} - \sqrt{V_f/\pi}\right)\right]\Delta T \tag{42}$$

The compression rate of NASC can be calculated by

$$R_c = \left(\frac{2}{\sqrt{2}E_f} + \frac{2t_i}{\sqrt{t_i^2 + 2t_i r_f}\,E_i}\right)\sigma_{cc}(t) + 2\int_{0^+}^{t} J_{cm}^T(t-\varsigma)d\varsigma\left(\frac{1}{2} - \frac{t_i\sqrt{V_f/\pi}}{r_f} - \sqrt{V_f/\pi}\right)\frac{\Delta\sigma_{cc}(t)}{\Delta t}$$
$$- \left[2\alpha_f\sqrt{V_f/\pi} + \frac{2\alpha_i t_i}{r_f}\sqrt{V_f/\pi} + 2\alpha_m\left(\frac{1}{2} - \frac{t_i\sqrt{V_f/\pi}}{r_f} - \sqrt{V_f/\pi}\right)\right]\Delta T \tag{43}$$

Substituting $\Delta T=0$ into Eq. (43) gives the compressive rate of NASC at room temperature. The compressive strain can be calculated by

$$\varepsilon_{cc} = \left(\frac{2}{\sqrt{2}E_f} + \frac{2t_i}{\sqrt{t_i^2 + 2t_i r_f}\,E_i}\right)\sigma_{cc}(t) + \left[X + Y(t)\right]\left(1 - \frac{2t_i\sqrt{V_f/\pi}}{r_f} - 2\sqrt{V_f/\pi}\right)\frac{\Delta\sigma_{cc}(t)}{\Delta t} \tag{44a}$$

$$-\left[2\alpha_f\sqrt{V_f/\pi}+\frac{2\alpha_i t_i}{r_f}\sqrt{V_f/\pi}+2\alpha_m\left(\frac{1}{2}-\frac{t_i\sqrt{V_f/\pi}}{r_f}-\sqrt{V_f/\pi}\right)\right]\Delta T \tag{44b}$$

where $X=\int_{0^+}^{t}J_{cm}^{T}(t-\varsigma)d\varsigma$ and $Y(t)=\int_{0^+}^{t}J_{cm}^{T}(t-\varsigma)d\varsigma$.

After unloading the compressive load, the residual compressive strain is

$$\varepsilon_{cb}=Y(t)\left(1-\frac{2t_i\sqrt{V_f/\pi}}{r_f}-2\sqrt{V_f/\pi}\right)\frac{\sigma_{cc}(t)}{t} \tag{45}$$

The resilient rate of NASC can be obtained by

$$R_c=\frac{\varepsilon_{bb}}{\varepsilon_{cc}} \tag{46}$$

where

$$\varepsilon_{bb}=\left(\frac{2}{\sqrt{2}E_f}+\frac{2t_i}{\sqrt{t_i^2+2t_i r_f}E_i}\right)\sigma_{cc}(t)+X(1-\frac{2t_i\sqrt{V_f/\pi}}{r_f}-2\sqrt{V_f/\pi})\frac{\Delta\sigma_{cc}(t)}{\Delta t}$$
$$-\left[2\alpha_f\sqrt{V_f/\pi}+\frac{2\alpha_i t_i}{r_f}\sqrt{V_f/\pi}+2\alpha_m\left(\frac{1}{2}-\frac{t_i\sqrt{V_f/\pi}}{r_f}-\sqrt{V_f/\pi}\right)\right]\Delta T \tag{47}$$

Substituting $\Delta T=0$ into Eq. (46) gives the resilient rate of NASC at room temperature.

5.2.6 Prediction of creep behavior
The creep behavior equation of NASC can be expressed by Eq. (48).

$$\varepsilon_{cc}(t)=\left(\frac{2}{\sqrt{2}E_f}+\frac{2t_i}{\sqrt{t_i^2+2t_i r_f}E_i}\right)\sigma_{cc}(t)+2\sigma_{cc}(0)J_{cm}^{T}(t)\left(\frac{1}{2}-\frac{t_i\sqrt{V_f/\pi}}{r_f}-\sqrt{V_f/\pi}\right)$$
$$-\left[2\alpha_f\sqrt{V_f/\pi}+\frac{2\alpha_i t_i}{r_f}\sqrt{V_f/\pi}+2\alpha_m\left(\frac{1}{2}-\frac{t_i\sqrt{V_f/\pi}}{r_f}-\sqrt{V_f/\pi}\right)\right]\Delta T \tag{48}$$

Because the strain in both fiber and interface is much smaller than that in matrix, only the strain in matrix is considered under compressive load. Then the stress-strain relationship of the third part in Fig.6 resulted from the resilience constitutive equation is in the form

$$\sigma_{cm}(t)=\varepsilon_{c2-3}(0)G_{cm}^{T}(t)+\int_{0^+}^{t}G_{cm}^{T}(t-\varsigma)\left[\frac{d\varepsilon_{c2-3}(\varsigma)}{d\varsigma}+\alpha_m\frac{dT(\varsigma)}{d\varsigma}\right]d\varsigma \tag{49}$$

If the compressive strain ε_{cc} is constant during the course of stress-resilience, Eq. (50) is obtained.

$$\sigma_{cm}(t)=\varepsilon_{c2-3}(0)G_{cm}^{T}(t)+\int_{0^+}^{t}G_{cm}^{T}(t-V)\alpha_m\frac{dT(V)}{dV}dV \tag{50}$$

The stress-resilience equation of NASC is in the form

$$\sigma_{cc}(t) = \frac{\varepsilon_{cc}(0)G_{cm}^{T}(t)}{1 - \dfrac{2t_i\sqrt{V_f/\pi}}{r_f} - 2\sqrt{V_f/\pi}} + \int_{0^+}^{t} G_{cm}^{T}(t-\varsigma)\alpha_m \frac{dT(\varsigma)}{d\varsigma}d\varsigma \qquad (51)$$

The detailed derivation of Eqs. (7)-(51) can be found elsewhere (Zhu, 2008).

6. Performance evaluation of NASC

6.1 Mechanical performances of non-asbestos sealing composites

The properties of NASC specified in current standards include mainly density, transverse tensile strength, plasticity, oil resistance, and so on. The performances of non-asbestos sealing gaskets can be divided into two types. One is related to the performance indexes of gasket products, which are the main items of product inspection prescribed in gasket product standards. These performance indexes are the important basis for evaluating the quality of gasket products. They involve compressibility, resilient rate, stress relaxation rate and leakage rate (AQSIQ, 2003; AQSIQ, 2008). The other is correlated with the gasket constants in current code design guidelines, such as gasket yield factor y which is defined as the minimum gasket stress required to cause the gasket material to deform into the flange face irregularities and gasket factor m which is defined as the ratio of the minimum gasket stress needed to hold the joint sealed under the operating conditions to the internal pressure p (ASME, 2007). In this section, the theoretic prediction and experimental evaluation of some performances of NASC and gasket products are presented.

6.1.1 Test apparatus and procedure

A series of tests for tensile property, compressibility, resilient rate, and stress relaxation property were conducted on an INSTRON 3367 universal testing machine. Samples were made of the developed NASC reinforced with aramid fiber, as mentioned in section 3.2.

For tensile tests, the dumbbell-shaped samples were adopted, and the tests were performed according to the Chinese standard GB/T 1447-2005 "Fiber-reinforced plastics composites/determination of tensile properties". The test conditions are listed in Table 8.

Sample Quantity	Sample Dimension (mm)	Fiber Length (mm)	Fiber Content (wt%)	Tensile speed (mm/min)	Temperature (K)
36	20×10×2.5	1-3, 4-6,7-9	5, 10, 15, 20, 30, 40	200	293, 373, 423

Table 8. The conditions for tensile tests

The compressibility and resilient rate tests were carried out according to the Chinese standard GB/T 12622-2008 "Standard test method for compressibility and recovery of gaskets for pipe flanges". The test conditions are listed in Table 9.

Sample Quantity	Sample Dimension (mm)	Fiber Content (wt%)	Loading Speed (mm/min)	The Maximum Stress (MPa)	Temperature (K)
8	10×10×2.5	20, 40	200	10, 20	293

Table 9. The conditions for compressibility and resilient rate tests

For the tests of the stress relaxation property, the samples were placed in the chamber of the testing machine and heated to the desired test temperatures. After the temperature remained constant for about 5 minutes, the compressive loads were applied to the samples. The change in compressive stress of the samples was measured over time under the constant sample deformation. The test conditions are listed in Table 10.

Sample Quantity	Sample Dimension (mm)	Fiber Content (wt%)	Loading Speed (mm/min)	The Maximum Stress (MPa)	Temperature (K)
8	10×10×2.5	20, 40	200	10, 20	293, 423

Table 10. The conditions for stress relaxation tests

6.1.2 Results and discussions

Figs. 17 and 18 show the stress-strain curves of the samples at room temperature with different fiber mean aspect ratios $\bar{\lambda}$ and fiber volume contents V_f, respectively.
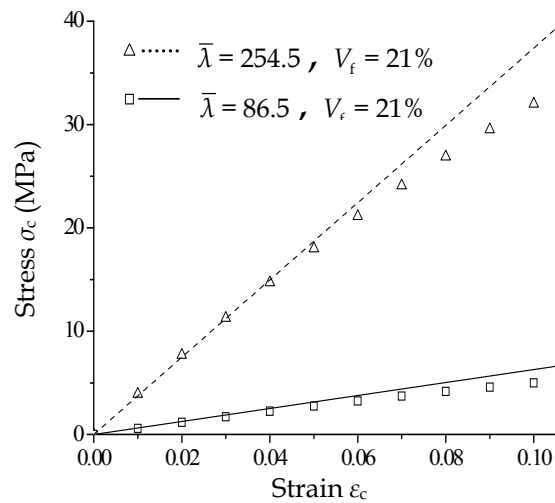
Fig. 17. Stress-strain curves of NASC with different fiber aspect ratios
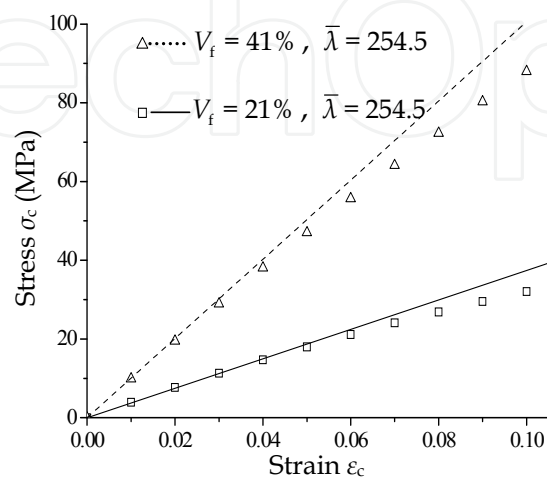
Fig. 18. Stress-strain curves of NASC with different fiber volume contents
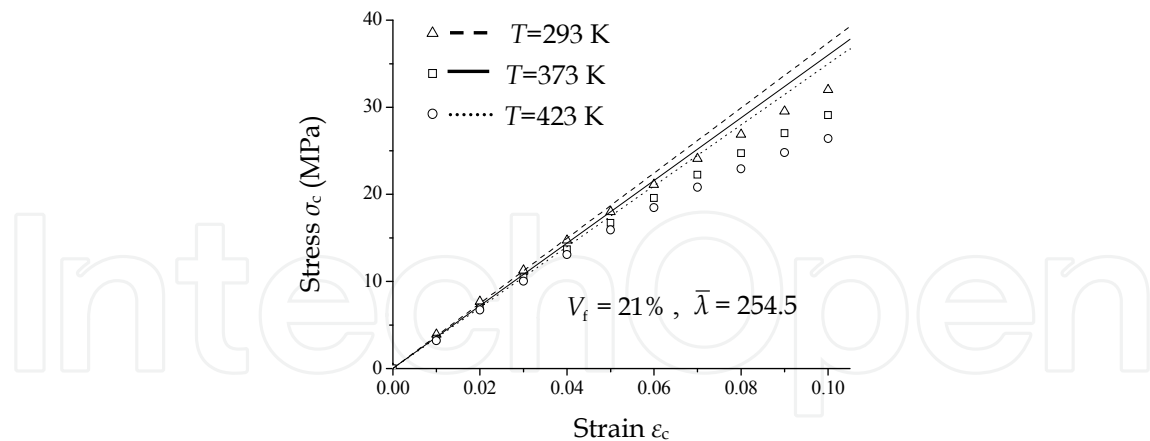
Fig. 19. Stress-strain curves of NASC at different test temperatures

Fig. 19 illustrates the stress-strain relationships of the samples at different test temperatures with a known fiber mean aspect ratio and a given fiber volume content. In these figures, symbols "Δ, □, o" represent experimental data, and the curves are plotted according to the prediction formulae proposed in section 5.2. It can be seen from the Figs. 17-19 that the slope of stress-strain curves of NASC increases with the increase of fiber mean aspect ratio and fiber volume content. Aramid fiber has a good reinforcing effect on elastomer matrix composites. The larger the fiber mean aspect ratio, the more obvious is the reinforcing effect. Because the modulus of aramid fiber is much larger than those of elastomer matrix material and compatibilization fiber like sepiolite fiber, the increase in the aramid fiber content results in the significant augment of the strength of NASC.

The error between the experimental data and values predicted using the derived constitutive equation increases with increasing strains, and all the predicted stresses are larger than those obtained by experiments. The essential reason for the error of prediction is that the difference between the aspect ratios of various fibers was neglected. The changes in the transverse tensile strength of NASC with fiber mean aspect ratio and fiber volume content are shown in Figs. 20-21.
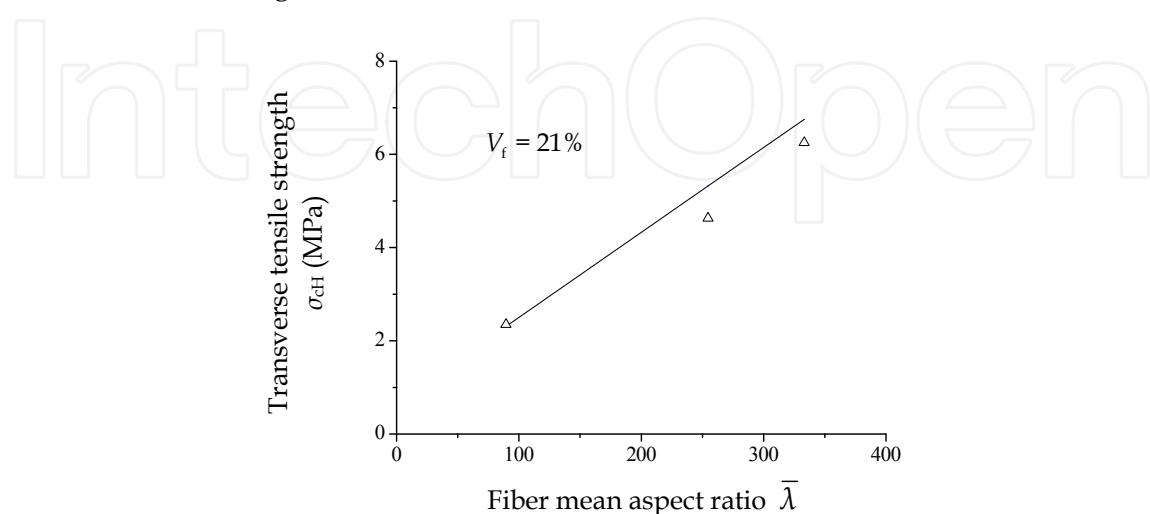
Fig. 20. Relationship between transverse tensile strength and fiber mean aspect ratio
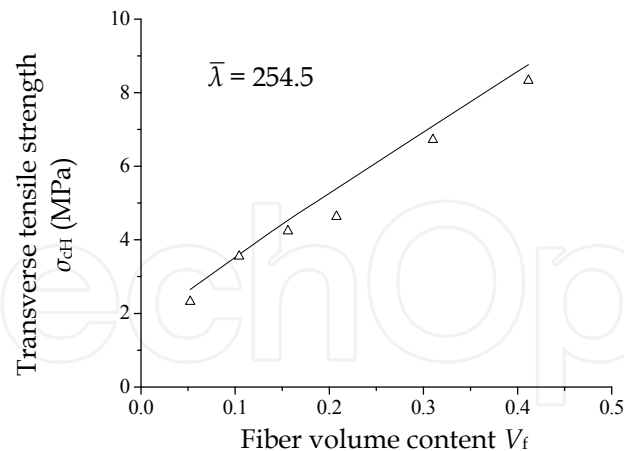
Fig. 21. Relationship between transverse tensile strength and fiber volume content

Fig. 22 illustrates the effect of test temperature on the transverse tensile strength. In these Figures, symbol "Δ" represents experimental data, and the curves represent the prediction results. The transverse tensile strength increases with the increase in the fiber mean aspect ratio and the fiber volume content. The transverse tensile strength of NASC is interrelated with temperature, and it deceases with increasing temperature. The temperature induces thermal stresses in the fiber, matrix and fiber-matrix interface, which affect the temperature-dependent tensile strength of the composite finally. Because the coefficient of thermal expansion of the elastomer matrix is much lager than that of the fiber, big thermal stresses both in the fiber and in the matrix will be generated with variation of temperature, and a small shear stress in the fiber-matrix interface is produced as well (Zhu et al., 2008). These factors result in the decrease of transverse tensile strength with increasing temperature.
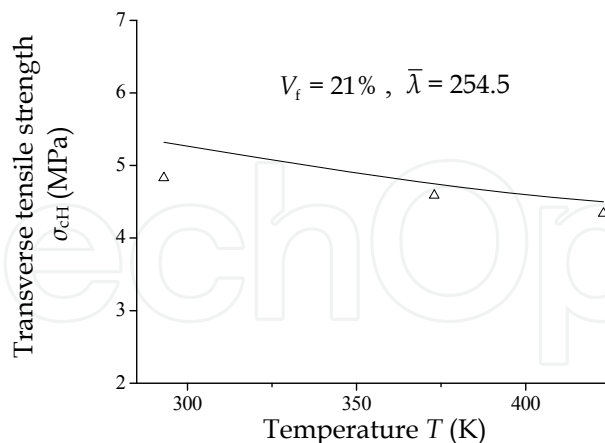
Fig. 22. Effect of temperature on transverse tensile strength

The compressibility and resilient rate of NASC obtained by tests and those predicted using Eqs. (43) and (46) are listed in Table 11. It can be found that the compressibility of NASC increases with increasing the maximum compressive stress and decreasing the fiber volume content, while the resilient rate decreases with the increase in the maximum compressive stress and the fiber volume content.

Fiber Content (wt%)	The Maximum Compressive Stress (MPa)	Compressibility (%)			Resilient Rate (%)		
		Test Data	Prediction Result	Relative Error (%)	Test Data	Prediction Result	Relative Error (%)
21	10	31.1	30.1	3.3	69.3	62.5	10.3
21	20	36.2	33.8	6.9	62.7	55.3	12.5
41	10	23.1	21.6	6.7	54.8	48.0	13.2
41	20	28.3	25.9	8.9	51.2	46.6	9.4

Table 11. Compressibility and resilient rate of NASC

Figs. 23-25 present the test and prediction results of stress relaxation property of NASC, in which symbols "Δ, □" represent experimental results, and the curves are plotted according to the prediction values of stress relaxation property using Eq. (51). The stress relaxation rate increases with increasing initial stress and temperature and decreasing fiber volume content. The fiber mean aspect ratio and orientation have less evident influence on the stress relaxation property of NASC. The experimental and prediction results are basically identical, and the maximum error is about 8.5%.
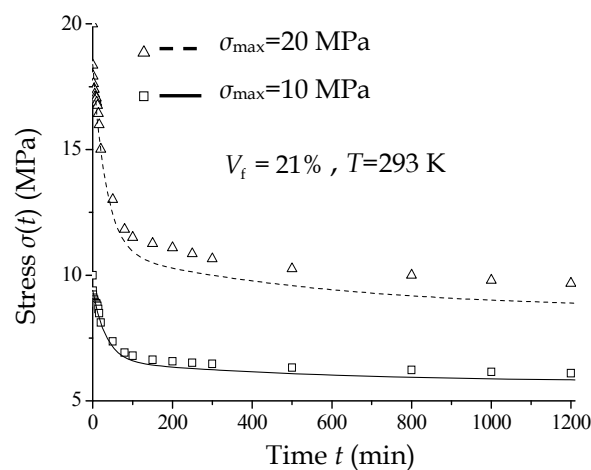
Fig. 23. Stress relaxation curves of NASC under different maximum stresses
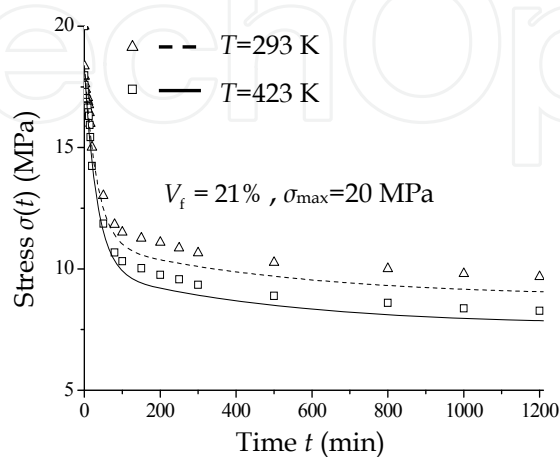
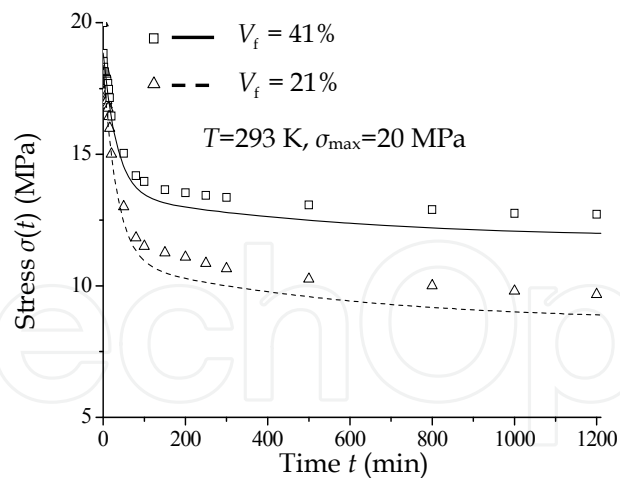Fig. 24. Stress relaxation curves of NASC at different temperatures

Fig. 25. Stress relaxation curves of NASC with different fiber contents

6.2 Sealing behaviour of non-asbestos sealing composites
6.2.1 Leakage model of non-asbestos gasket sealing

NASC can be assumed to be a kind of porous media. The flow of gas through porous media includes molecular transfer and convection transfer. The leakage rate L of gases flowing through porous media can be calculated using the capillary model (Gu et al., 2007b).

$$L = \sum_{i=1}^{k} \left(\frac{\pi r_i^4}{8\eta c l_m} p_m + \frac{4r_i^3}{3c l_m} \sqrt{\frac{2\pi RT}{M}} \right) (p_1 - p_2) \tag{52}$$

where r_i and l_m are the radius and the average length of capillaries, respectively, c is the bending coefficient of capillaries, η the dynamic viscosity of gases, T the Kelvin temperature of gases, M the gas molecular weight, R the gas constant, p_m the average pressure, $p_m=(p_1+p_2)/2$, and p_1 and p_2 are the pressures at the entrance and exit of capillaries, respectively.

There exists the following relationship between the number k and the radius r_i of leakage paths and the gasket compressive stress σ:

$$k = f_1\left(\sigma^{-m}\right) \tag{53}$$

$$r_i = f_2\left(\sigma^{-n}\right) \tag{54}$$

According to Eqs.(52)-(54), the leakage rate of gas through gasket sealing joints L can be calculated by the following formula:

$$L = \left[A_L \frac{1}{\eta} \left(\frac{\sigma}{\sigma_0} \right)^{-n_L} p_m + A_M \sqrt{\frac{T}{M}} \left(\frac{\sigma}{\sigma_0} \right)^{-n_M} \right] \frac{(p_1 - p_2)}{l} \tag{55}$$

where l is the gasket effective width, A_L, A_M, n_L and n_M are regression coefficients which can be obtained from experimental data, and σ_0 is the gasket seating stress prescribed in the corresponding gasket standards (AQSIQ,2003, AQSIQ,2008).

6.2.2 Test verification and leakage rate prediction method

Tests were performed on a fully automatic testing machine for gasket performances, and the specific details on the test machine and test procedure can be found in the reference (Gu et al., 2007b). The test conditions are listed in Table 12.

Sample Quantity	Sample Dimension (mm)	Test Medium	Gasket Seating Stress (MPa)	Gas Pressure Difference (106 Pa)	Test Temperature (K)
3	$\phi 109 \times \phi 61 \times 2$	99.9% nitrogen	20, 30, 40, 50, 60	1, 2, 3, 4.5, 6	293

Table 12. Conditions for the leakage test

The relationship between medium pressure difference p_1–p_2 and leakage rate L under different gasket seating stresses σ_S is shown in Fig. 26, in which symbols represent experimental data, and curves are plotted according to the leakage model. The experimental results show that the leakage rate increases obviously with the increase of the test medium pressure when the gasket seating stresses are smaller. On the contrary, when the gasket seating stresses are larger, this tendency is not obvious. The variation of leakage rates with pressure difference across gasket width follows precisely the curves represented by the leakage model, as indicated by the high value of the correlation coefficient R which is nearly equal to unity.
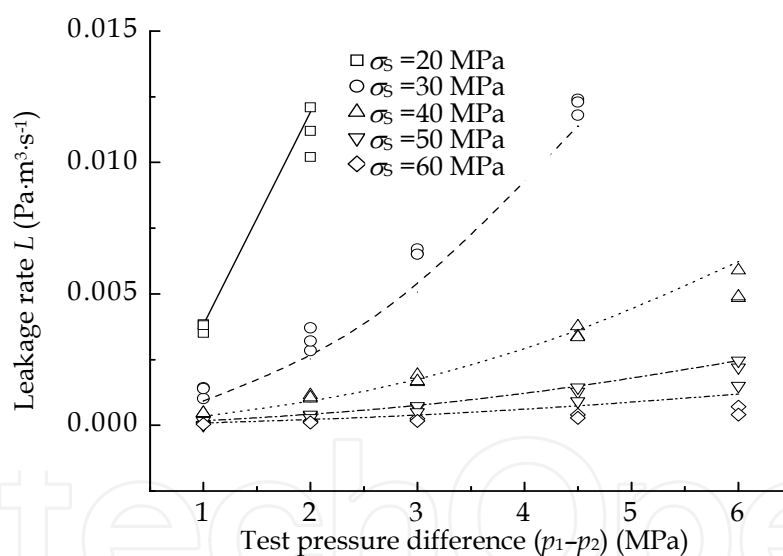

Fig. 26. Relationship between leakage rate and test pressure difference under different seating stresses

The coefficients A_L, A_M, n_L and n_M in Eq. (55) can be obtained by regression analysis of the experimental data, and they are listed in Table 13. According to Eq. (55) and the regression coefficients, the relationships between the pressure difference and the leakage rate under different gasket compressive stresses are obtained, and they are also illustrated in Fig. 26.

A_L	A_M	n_L	n_M	R
8.52×10^{-23}	2.79×10^{-12}	4.08	3.06	0.984

Table 13. Regression coefficients in Eq. (55)

According to Eq. (55) and the regression coefficients in Table 13, the leakage rates of other gases leaking through non-asbestos gaskets with different sizes and used under various working conditions can also be predicted. It can be assumed that the leakage paths in gaskets are distributed uniformly in the circumferential direction. The larger the gasket perimeter, the more the leakage paths are. Therefore, when the leakage rate prediction is performed for the gaskets with different sizes, the correction of Eq. (56) is necessary, and hence, the leakage prediction formula holds:

$$L = \left[A_L \frac{1}{\eta} \left(\frac{\sigma}{\sigma_0} \right)^{-n_L} p_m + A_M \sqrt{\frac{T}{M}} \left(\frac{\sigma}{\sigma_0} \right)^{-n_M} \right] \frac{(p_1 - p_2)}{l} \frac{D_2}{D_1} \tag{56}$$

where D_1 and D_2 are diameters of the tested gasket and the gasket on which the leakage rate will be predicted, respectively.

It can be seen from Eq. (55) and Eq. (56) as well that the total leakage rate of gases through non-asbestos gaskets is the sum of the laminar flow rate and the molecular flow rate. The leakage is mainly the molecular flow when the gasket seating stress is large and the gas pressure is low, and the leakage rate is directly proportional to the pressure difference (p_1-p_2). On the contrary, when the gasket seating stress is small and the gas pressure high, the leakage is predominantly the laminar flow. In this case, the leakage rate is in direct proportion to the square difference of pressures (p_1^2-p_2^2), and the influence of the molecular flow can be ignored. The latter situation represents the leakage state of gasket sealing joints in most pressure vessels and piping.

7. Conclusions

Two kinds of non-asbestos sealing composites were developed by using aramid, glass, and pre-oxidized carbon fibers as reinforcing fibers, and nitrile rubber and natural rubber as binders. Design of these composites as well as preparation techniques were discussed. The surface treatment effects of fibers by using such methods as immersion coating, surface oxidation and plasma treatments were investigated. The results of the transverse tensile test and the SEM analysis reveal that the surface pretreatment can largely enhance the associative strength of the interface between fiber and matrix.

Both the molding and the calendaring preparation processes of NASC were presented. Contents of main compositions of two kinds of NASC were determined by uniform design and regression design methods in which the transverse tensile strength, compressibility, resilient rate and stress relaxation rate of the composites were used as evaluation indexes. According to the data resulted from mixing regression design experiments, the regression equation was obtained.

Methods for measuring and characterizing the micro structural parameters including the aspect ratio, orientation, distribution of short fibers, interphase thickness, and porosity of NASC were discussed. The short fiber aspect ratio can be obtained by measuring the dimensions of the fibers that were separated from the composite, and results can be evaluated by the mean aspect ratio method, the histogram method and the distribution function method. The short fiber orientation can be tested by the section-analysis method and the plane-observation method, and results can be evaluated by the distribution function method, the histogram method and the modified coefficient method.

The micromechanical model of a single fiber cylindrical cell, which includes fiber, matrix and their interphase, was established. The stress transfer mode among the fiber, the matrix and the interphase was investigated, and the stress distributions in them were obtained. A model of a compressive type single-fiber cell was established, and the prediction methods for the stress-strain relationship, the tensile module, the longitudinal tensile strength, the transverse tensile strength, the compression-resilience performance and the creep behavior were proposed.

A series of tests for tensile property, compressibility, resilient rate, and stress relaxation property of NASC were conducted. The experimental results were compared with the predicted values. The predicted stress-strain relationship of NASC is in good agreement with the experimental result when the strain of the composite is relatively small, while the error is obvious when the strain is relatively large. The transverse tensile strength increases with the increase of the fiber volume content and the mean aspect ratio and decreases with the increase in the test temperature. All the experimental results are smaller than those predicted, and the maximum error between them is about 13%. The compressibility increases with increasing the maximum compressive stress and decreasing the fiber volume content, while the resilient rate decreases with the increase in the maximum compressive stress and the fiber volume content. They are nearly irrelevant to the fiber mean aspect ratio and orientation. The errors both between the predicted compressive rates and experimental data and between the predicted resilient rates and the experimental results are less than 15%. At the beginning of the stress relaxation, the stress in the composite decreases quickly, the stress relaxation speed decreases essentially after 80 to 100 minutes, and the stress relaxation curve trends to be a straight line. The stress relaxation rate increases with increasing initial stress and temperature and decreasing fiber volume content. Such microstructure parameters as fiber mean aspect ratio and orientation have less evident influence on the stress relaxation property of NASC. The experimental and predicted results are basically identical, and the maximum error is about 8.5%, which indicates that the stress relaxation property of NASC can be well evaluated by the stress relaxation equation presented in this chapter.

A leakage model was developed to predict non-asbestos gasket leakage rates with different gasket sizes and various gases under different working conditions. The model is constructed on the base of the gasket leakage tests conducted over a nitrogen pressure range of 1 to 6 MPa and a gasket seating stress range of 20 to 60 MPa. The established model gives relatively accurate predictions, but it is necessary to conduct additional tests before predicting leakage rate of other types of gaskets. High temperature will cause the deterioration of sealing materials and result in the increase of leakage rates, which has not been taken into consideration in the present model, and this subject should be studied.

8. Acknowledgement

9. References

American Academy of Actuaries (2007). *Overview of Asbestos Claims Issues and Trends*, Mass Torts Subcommittee of the American Academy of Actuaries, Washington, USA

AQSIQ (2003). The General Administration of Quality Supervision, Inspection and Quarantine of the People's Republic of China, GB/T 9129-2003, *Specifications of Non-metallic Flat Gaskets for Pipe Flanges*. Standards Press of China, ISBN 155066.1-19884, Beijing, China (in Chinese)

AQSIQ (2008). The General Administration of Quality Supervision, Inspection and Quarantine of the People's Republic of China, GB/T 17727-2008, *Nonmetal material gaskets for marine flange*. Standards Press of China, ISBN 750665591, Beijing, China (in Chinese)

ASME (2007). The American Society of Mechanical Engineers, *ASME Boiler and Pressure Vessel Code 2007, Sec VIII, Division 1, Rules for construction of Pressure Vessels*. New York, USA

Chen, Y. & Gu B.Q. (2008). Development of a new kind of sealing composite material reinforced with carbon and glass hybrid fibers. *Advanced Materials Research*, Vols. 44-46, 651-658, ISSN 1022-6680

Gao, P. & Chen Y. (2009). The effect of nanometer modification on the performances of short fiber reinforced rubber-based sealing composite material. *Lubrication Engineering*, Vol.34, No.8, 66-69, ISSN 0254-0150 (in Chinese)

Gu B. Q. & Chen, Y. (2007). Development of a new kind of sealing composite material reinforced with aramid and pre-oxidized fibers. *Key Engineering Materials*. Vols. 353-358, 1243-1246, ISSN 1013-9826

Gu, B. Q. (1999). Application of model of gases flowing through porous media to gasket sealing. *Journal of Nanjing University of Chemical Technology*, Vol. 21, No. 1, 19-22, ISSN 1007-7537 (in Chinese)

Gu, B. Q., Shi, L. X. & Lu, X. F. (2000). Investigation of high temperature performances of spiral wound gaskets with flexible graphite filler. *China Petroleum Machinery*, Vol. 28, No. 2, 13-16, ISSN 1001-4578 (in Chinese)

Gu, B. Q., Lu, X. F. & Xu, G. P. (2001). Determination of performance indexes of non-asbestos fiber-reinforced elastomer gasket. *Proceedings of the 5th National Conference on Pressure Vessel Technology*, 116-120, ISSN 1007-7472.0.2000-05-023, Nanjing, China, Setember, 2001, Subcommittee on Pressure Vessels, Chinese Society of Mechanical Engineers, Hefei, China (in Chinese)

Gu, B. Q. (2002). Performances and application of non-asbestos gaskets. *Process Equipment & Piping*, Vol. 39, No. 1, 5-9, ISSN 1009-3281 (in Chinese)

Gu, B. Q., Li, Y. Y., Sun, Z. G., Huang, X. L., Zhou, J. F. & Shao, C. L. (2010). Study on time-correlated leakage model of nonmetallic gaskets. *Advanced Materials Research*, Vols. 97-101, 629-633, ISSN 10226680

Gu, B. Q. & Zhu, H. S. (1988). Tightness analysis of bolted flanged connections. *Petro-chemical Equipment*, Vol. 17, No. 1, 16-20, ISSN 1000-7466 (in Chinese)

Gu, B. Q. & Huang, X. L. (1997). Dichtheitsklassen und entsprechende Leckratenmeßverfahren. *3R international*, 1997, Vol.36, No.4/5,198-201, ISSN 0340-3386

Gu, B. Q., Li, X. H. &Tian, Z. (2004). *Static seal design Technology.* Standards Press of China, ISBN 7-5066-3430-9, Beijing, China (in Chinese)

Gu, B. Q. & Chen, Y. (2006). Tightness assessment method of bolted flanged connections at elevated temperature. *Lubrication Engineering*, Vol. 178, No. 6, 39-41, ISSN 0254-0150 (in Chinese)

Gu, B. Q., Chen, Y., Zhang, Y. & Zhu, R. S. (2007a). Tightness prediction of flanged joints with elastic washers. *Proceedings of the Ninth International Conference on Engineering Structural Integrity Assessment*, 1512-1515, ISBN 978-7-111-05002-5, Beijing, China, October, 2007, China Machine Press, Beijing, China

Gu, B. Q., Chen, Y. & Zhu, D. S. (2007b). Prediction of leakage rates through sealing connections with nonmetallic gaskets. *Chinese Journal of Chemical Engineering*, Vol. 15, No. 6, 837-841, ISSN 1004-9541

Marchand, L., Derenne, M. (1996). Long term performance of elastomeric sheet gasket materials subjected to temperature exposure. *Proceedings of the International Conference on Pressure Vessel Technology*, 107-123, ISBN 079181789X, Montreal, Can, July, 1996, ASME, New York, NY, USA

Payne, J. & Bazergui, A. (1990). *Summary Report on Elevated Temperature Tests for Asbestos-free Gasket Materials*, NACE for MTI., ISBN 1-877914-10-X

Payne. J. R., Mueller, R. T., Bazergui, A. (1989a). Gasket qualification test scheme for petrochemical plants. Part I. Test methods and application results. *Application of Modal Analysis Techniques to Seismic and Dynamic Loadings*, Vol. 158, 53-58, ISSN 0277027X, Honolulu, HI, USA, July, 1989, ASME, New York, NY, USA; JSME, Tokyo, Jpn

Payne. J. R., Mueller, R. T., Bazergui, A. (1989b). Gasket qualification test scheme for petrochemical plants. Part II. Quality criteria and evaluation schemes. *Application of Modal Analysis Techniques to Seismic and Dynamic Loadings*, Vol. 158, 59-69, ISSN 0277027X, Honolulu, HI, USA, July, 1989, ASME, New York, NY, USA; JSME, Tokyo, Jpn

Piringer, S. & Rustemeyer U. (2004). Improving performance of fiber-based gaskets at elevated temperatures-the sandwich approach. *Sealing Technology*, Vol. 2004, No. 3, 6-11, ISSN 1350-4789

Tsuji, H., Kitagawa, H., Kodaira, N. (2004). Effect of aging time on sealing performance of non-asbestos gasket at elevated temperature. *Analysis of Bolted Joints*, 209-214, ISBN 0791846814, San Diego, CA, United States, July, 2004, ASME, New York, NY, USA

Xie, S. J. & Cai R. L. (2002). Research on mechanical behaviour of the compressed nonasbestos fiber reinforced rubber sheet. *Fluid Machinery*, Vol. 30, No. 12, 4-6, ISSN 1005-0329 (in Chinese)

Xie, S. J. & Xie, J. M. (2004). Investigation into the effect of nonasbestos fibers on the performances of compressed nonasbestos sealing sheets. *Non-Metallic Mines*, Vol. 27, No. 1, 50-52, ISSN 1000-8098 (in Chinese)

Zhu, D. S., Gu, B. Q. & Chen, Y. (2007). Study on Tensile Strength of Short-fiber-reinforced elastomer matrix composites. *Proceedings of the Ninth International Conference on Engineering Structural Integrity Assessment*, 803-807, ISBN 978-7-111-05002-5, Beijing, China, October, 2007, China Machine Press, Beijing, China

Zhu, D. S., Gu, B. Q. & Chen, Y. (2008). Study on Temperature-Dependent Tensile Strength of Short-Fiber-Reinforced Elastomer Matrix Composites. *Advanced Materials Research,* Vols. 44-46, 97-104, ISSN 1022-6680

Zhu, D. S. (2008). Prediction of Mechanical Performances of Short Fiber Rubber Matrix Composite. A dissertation for the doctoral degree at Nanjing University of Technology (in Chinese)
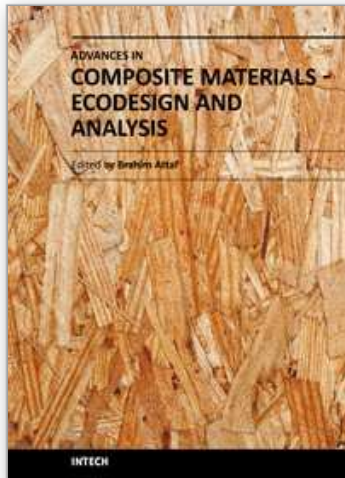
Advances in Composite Materials - Ecodesign and Analysis

Edited by Dr. Brahim Attaf

By adopting the principles of sustainable design and cleaner production, this important book opens a new challenge in the world of composite materials and explores the achieved advancements of specialists in their respective areas of research and innovation. Contributions coming from both spaces of academia and industry were so diversified that the 28 chapters composing the book have been grouped into the following main parts: sustainable materials and ecodesign aspects, composite materials and curing processes, modelling and testing, strength of adhesive joints, characterization and thermal behaviour, all of which provides an invaluable overview of this fascinating subject area. Results achieved from theoretical, numerical and experimental investigations can help designers, manufacturers and suppliers involved with high-tech composite materials to boost competitiveness and innovation productivity.

How to reference

In order to correctly reference this scholarly work, feel free to copy and paste the following:

Boqin Gu, Ye Chen and Jianfeng Zhou (2011). Design, Manufacture and Performance Evaluation of Non-Asbestos Sealing Composites, Advances in Composite Materials - Ecodesign and Analysis, Dr. Brahim Attaf (Ed.), ISBN: 978-953-307-150-3, InTech, Available from: http://www.intechopen.com/books/advances-in-composite-materials-ecodesign-and-analysis/design-manufacture-and-performance-evaluation-of-non-asbestos-sealing-composites

INTECH
open science | open minds